VTL-PUB-71
DECEMBER, 1980

E-546

A Study of the Momentum Distributions of the Final State Hadrons in Neutrino-Nucleus Interactions

by

Gregory M. Swider

FERMILAB
DEC 26 1980
LIBRARY

AAB1980

University of Washington

Abstract

A STUDY OF THE MOMENTUM DISTRIBUTIONS OF THE FINAL STATE HADRONS IN NEUTRINO-NUCLEUS INTERACTIONS

by Gregory M. Swider

Chairperson of the Supervisory Committee:

Thompson H. Burnett
Department of Physics

In an experiment using the Fermilab 15-foot Bubble Chamber/Two-Plane EMI with a 47 percent (atomic) neon-in-hydrogen fill exposed to the quadrupole-triplet neutrino beam, we have identified some 9600 neutrino charged-current events. We have measured approximately 4000 of these, one quarter of which were especially selected for having higher $-q^2$ values. We have undertaken the study of the momentum distributions of the produced hadrons, comparing them with a model based on phase space and a model based on the Field and Feynmann fragmentation scheme. The longitudinal momentum distributions, as parameterized by the fragmentation functions, are in reasonable agreement with both models. A mild softening of these distributions with increasing $-q^2$ is evident, especially in the positive hadrons. Transverse momenta are reasonably well reproduced by the models at lower values, but the data exhibit an excess of hadrons at higher p_t not indicated in either model. This high p_t excess is particularly pronounced in the higher $-q^2$ or higher W events; the low $-q^2$ and low W events agree with the models for all values of p_t.

We have examined the transverse momentum distributions separately for the forward jet hadrons and the backward jet hadrons, where the separation is made based on the longitudinal momentum fraction determined in the hadronic center-of-mass frame. We observe that the high p_t excess is clearly associated with the forward jet hadrons, while the backward jet hadrons agree with phase space for the full p_t range. Fitting exponentials to the p_t distributions, there is a significant change in the "slope" parameter for the forward jet hadrons in going from low to high $-q^2$ (or low to high W); no statistically significant change is evident in the backward jet hadrons' distributions. This high p_t - forward jet correlation is displayed well in plots of the average values of p_t^2 and their dependence on $-q^2$ and W; a rise with rising $-q^2$ or rising W is evident for the forward jet, but only the rise indicated by phase space is evident in the backward jet. Plotting average p_t^2 versus the longitudinal momentum fraction (in the hadronic center-of-mass), the "seagull" plot, we observe a definite forward-backward asymmetry for higher $-q^2$ (W) events. An attempt to separate the effects of $-q^2$ and W for p_t is inconclusive, but the

majority of the distributions shown favor W as the more important of the two variables.

A discussion of these effects in terms of the two models concludes that the departures of the data from phase space are not explainable by either of the two models considered. QCD, however, is in at least qualitative agreement with all of these results; moreover, a comparison of our p_t distributions with an analytic calculation based on QCD gives encouraging agreement.

TABLE OF CONTENTS

Chapter I: Introduction 1

Chapter II: Experimental Arrangement 6
Data Collection. 6
Data Reduction 12

Chapter III: Theory 16
Charged Current Neutrino-Nucleon Scattering. . .16
Hadronic Final State 19
Models of Hadronization; Longitudinal Phase Space 22
Field and Feynman Model 24
Quantum Chromodynamics 26

Chapter IV: Data Analysis and Presentation 31
Event Selection and Measurement. 31
Monte Carlo Simulation 32
Energy Estimation. 32
Multiplicities 37
Momentum Distributions 46
Longitudinal Momentum. 46
Transverse Momentum. 57
Correlations Between Longitudinal and Transverse Momentum. 65
Experimental Biases. 87

Chapter V: Conclusions. 97

List of References 106

Appendix A: The Two-Plane External Muon Identifier. . 109

Appendix B: Selection of Event Sample and Analysis Procedures 112
Charged Current Event Identification 112
Selection of Analysis Sample 113
Event Measurement. 114
Analysis Specifications. 116

Appendix C: Monte Carlo Simulation. 123
Longitudinal Phase Space 126
Field and Feynman Model. 127

LIST OF TABLES

Number Pages

4-1: Fits of hadronic multiplicities. 45

4-2: Fits of the transverse momentum 74

LIST OF FIGURES

Number — Page

2-1. Experimental apparatus; Main Ring, Neutrino Beam Line, 15-foot Bubble Chamber/Two-Plane EMI 8

2-2. Neutrino energy spectrum for the Quadrapole Triplet beam[II-1] 9

2-3. 15-foot Bubble Chamber/2 Plane EMI 10

2-4. Schematic of the EMI with associated data collection electronics 13

3-1. Figurative depiction of the scattering process 17

4-1. Distribution of the hadronic energy correction factor, "g". 34

4-2. Distribution of (corrected) event energy for the analysis sample. The LPS and FF model distributions (normalized to the data) are superimposed. 36

4-3. Distribution of $Q^2 = -q^2$ for the analysis sample, with the LPS and FF model curves superimposed.. 38

4-4. Distribution of W^2 for the analysis sample 39

4-5. Distribution of x for the analysis sample 40

4-6. Distribution of y for the analysis sample 41

4-7. Multiplicities of charged hadrons versus the logarithm of $-q^2/M^2$ and W^2/M^2.. 42

4-8. Distribution of $D^+(z)$ and $D^-(z)$ for all hadrons; 4-8a uses $z = z_+$, 48b uses $z = z_-$ 43

4-9. Distribution of $D^+(z)$ and $D^-(z)$ for $z = z_{vis}$ 49

Number — Page

4-10. Distribution of $D^+(z_+)$ for low and high $-q^2$ events 50

4-11. Distribution of $D^-(z_+)$ for low and high $-q^2$ events 51

4-12. Distribution of $D^+(z_+)$ for low and high W^2 events 53

4-13. Distribution of $D^-(z_+)$ for low and high W^2 events 54

4-14. Distribution of $D^+(z_+)$ for low and high $-q^2$ events, for all events with $x > 0.3$ 55

4-15. Distribution of $D^+(z_+)$ for low and. . . . . high W^2 events, for all events with $x > 0.3$ 56

4-16. Distribution of transverse momentum (squared), measured from both the VHD and the LP, for all hadrons 59

4-17. Distribution of transverse momentum (squared) from the VHD for all hadrons, events separated into low and high $-q^2$. . . 60

4-18. Distribution of transverse momentum (squared) from the VHD for all hadrons events separated into low and high W^2 . . . 61

4-19. Average transverse momentum (squared) versus $-q^2$; 4-19a is p_t measured from the LP, 4-19b that measured from the VHD. . 63

4-20. Average transverse momentum (squared) versus W^2; 4-20a is p_t measured from the LP, 4-20b that measured from the VHD . . . 64

4-21. Distribution of transverse momentum (squared) from the VHD for the forward jet hadrons and the backward jet hadrons. . 67

4-22. Distribution of transverse momentum (squared) from the VHD for the forward jet hadrons and backward jet hadrons separately 68

Number Page

4-23. Distribution of transverse momentum (squared) from the VHD for the forward jet hadrons, events separated into low and high $-q^2$. 69

4-24. Distribution of transverse momentum (squared) from the VHD for the jet hadrons, events separated into low and high W^2 70

4-25. Distribution of transverse momentum (squared) from the VHD for the backward jet hadrons, events separated into low and high $-q^2$. 71

4-26. Distribution of transverse momentum (squared) from the VHD for the backward jet hadrons, events separated into low and high W^2 72

4-27. Average transverse momentum squared versus $-q^2$ for the forward jet hadrons and the backward jet hadrons; 4-27a is p_t from the LP, 4-27b is p_t from the VHD. 75

4-28. Average transverse momentum squared versus W^2 for the forward jet hadrons and the backward jet hadrons; 4-28a is p_t from the LP, 4-28b is p_t from the VHD. . 76

4-29. Average transverse momentum squared versus $-q^2$ for three minimum values of z_+ . 78

4-30. Average transverse momentum squared versus W^2 for three minimum values of z_+. . 79

4-31. Average transverse momentum squared versus $-q^2$ for three minimum values of z_- . 80

4-32. Average transverse momentum squared versus W^2 for three minimum values of z_-. . 81

4-33. Seagull versus $-q^2$; average transverse momentum squared versus z_+ and z_-, events separated into low and high $-q^2$ 82

4-34. Seagull versus W^2; average transverse momentum squared versus z_+ and z_-, events separated into low and high W^2. 83

Number Page

4-35. Average transverse momentum squared versus $-q^2$ for the forward jet hadrons, events with $W^2 < 45$ $(GeV/c^2)^2$; 4-35a is for p_t from the LP, 4-35b for p_t from the VHD. 85

4-36. Average transverse momentum squared versus W^2 for the forward jet hadrons, events with $-q^2 < 15$ $(GeV/c^2)^2$; 4-36a is for p_t from the LP, 4-36b for p_t from the VHD 86

4-37. Average transverse momentum squared versus $-q^2$ for the forward jet hadrons, events with $W^2 > 45$ $(GeV/c^2)^2$; 4-37a is for p_t from the LP, 4-37b for p_t from the VHD. 88

4-38. Average transverse momentum squared versus W^2 for the forward jet hadrons, events with $-q^2 > 15$ $(GeV/c^2)^2$; 4-38a is for p_t from the LP, 4-38b for p_t from the VHD 89

4-39. Distribution of the transverse momentum of the total hadronic system from the Lepton Plane 92

5-1. Distribution of transverse momentum (squared) from the VHD for all hadrons, separated into low and high $-q^2$, with analytic QCD predicted curves superimposed. 100

5-2. Distribution of transverse momentum (squared) from the CHD for all hadrons, separated into low and high W^2, with analytic QCD predicted curves superimposed. 101

ACKNOWLEDGMENTS

I wish to express my appreciation to my parents for providing me with the background and motivation that has culminated in this dissertation and this degree.

CHAPTER I

INTRODUCTION

"Neutrinos, they are very small
They have no charge and have no mass
And do not interact at all.
The earth is just a silly ball
To them, through which they simply pass,
Like dustmaids down a drafty hall
Or photons through a sheet of glass.
They snub the most exquisite gas,
Ignore the most substantial wall,
Cold shoulder steel and sounding brass,
Insult the stallion in his stall,
And, scorning barriers of class,
Infiltrate you and me. Like tall
And painless guillotines they fall
Down through our heads into the grass.
At night, they enter at Nepal
And pierce the lover and his lass
From underneath the bed - you call
It wonderful; I call it crass." [I-1]

This thesis concerns itself with the collection and analysis of data from an experiment involving neutrino interactions with nuclei. The specific processes of the data to be examined are the characteristics of the hadronic system that results, i.e. what happens to the struck nucleon after the neutrino scatters with it. Moreover, this study will focus on the dependence of this hadronic system on the depth within the nucleon that the neutrino penetrates when it scatters.

The study of hadronic physics has been greatly facilitated through the use of deep inelastic lepton-nucleon scattering experiments [I-2]. The primary virtue of such experiments is that the behavior of the lepton is well

understood, and that the lepton is (relatively) identifiable. Measuring the momentum of the lepton(s) before and after the scatter tells us the momentum transferred to the nucleon, and the knowledge of leptonic interactions tells us the manner in which it was delivered. Collecting data for a wide range of momentum transfers permits the systematic study of the behavior of the structure of the nucleon when probed in this fashion.

One of the first discoveries of such experiments is that the entire nucleon is not the target [I-3]. That is, varying the momentum transferred to the nucleon in a fashion that varies the distance over which the transfer occurs indicates that the scatter can take place between the lepton and a substructure within the nucleon. And, in that the result of such a scatter often consists of several hadrons being produced, the following hypothesis is suggested: the substructure within the nucleon that scatters with the lepton is not a hadronic entity that typically exists alone, separate from other hadronic matter; it is usually bound within a nucleon or other hadron. However, when violently ejected from the nucleon by the lepton, both this constituent and the nucleon remnant are driven toward this isolated condition. This state is avoided because the same forces that bound the constituent and the nucleon remnant together before now attempt to rebind them into hadrons, a process that often produces a collection of hadrons as well as those that now contain the original constituent and nucleon remnant. The

energy for producing these several hadrons comes from the lepton; the momentum transferred is shared among the newly created particles as well.

Previous experiments have studied such fragmentation of the struck constituent and nucleon remnant into the several hadrons. They have measured the momentum distributions, and have determined that the hadrons' momenta are basically collinear. The longitudinal and transverse momentum components have been studied separately, and the dependence of these distributions on the momentum transfer, total hadronic energy, etc. has been investigated. In this study, we will continue and extend such analyses. We will examine the momentum distributions of the hadrons in terms of the components, and will investigate the dependence on total hadronic energy, etc. over a wider range of such variables than most previous experiments accessed. We will investigate the correlations between the longitudinal and transverse momentum components, something that only recently has received any attention. Moreover, we will perform such analysis separately for those produced hadrons that are associated with the struck constituent and for those associated with the nucleon remnant, an aspect of this phenomenon that has not previously been studied.

The use of a neutrino beam in a heavy liquid bubble chamber permits the study of the details of the outgoing hadrons produced from a scatter in which a measureable amount of momentum and energy are transferred to the nucleon.

The neutrino beam is vital in that it can yield as high or higher energy data as can be obtained in other deep inelastic scattering experiments. Specifically, much harder scatters can be observed (harder in the sense of scattering over very short times and distances and involving high momentum transfers), than can be obtained in charged lepton scattering [I-4]. The use of a bubble chamber enables analysis of the hadronic system more extensive than other data collection systems can achieve. This study will, for example, concentrate on the comparisons of the lower momentum hadrons with the higher momentum ones, and the ability of the bubble chamber to measure both with high resolution is critical. For these reasons these data permit investigation of aspects of hadronic processes that have previously not been amenable to careful study.

In the following sections we will discuss some of the details of the data collection and analysis procedures that resulted in this study. We will then briefly outline some of the relevant theoretical topics and models that we will want to compare with aspects of the data. We will then present various distributions concerning the manner in which the available momentum and energy is distributed among the several final state hadrons. We will conclude by reviewing the data as they pertain to the theory, investigating how the results of the analysis may support or refute current beliefs in the understanding of hadronic processes.

NOTES TO CHAPTER I

I-1 J. Updike, "Cosmic Gall," Telephone Poles and Other Poems, Alfred A. Knopf, Inc. (1960)

I-2 The number of articles referring to this topic is enormous; for a discussion of the early studies of nucleon structure using lepton probes, see A. DeRujula, et al., Rev. Mod. Phys. 46, 391 (1974) and references contained therein; more recent results on structure functions can be found in F. Sciulli, talk given at the XX International Conference on High Energy Physics, Madison (July, 1980); references on the hadronic final state are cited where appropriate in subsequent sections.

I-3 Again, the number of references that relate to the general features of deep inelastic scattering data is quite large; however, a reasonably complete summary of earlier results, relevant to this discussion, can be found in the publication by D. H. Perkins, Rep. Prog. Phys. 40, 409 (1977)

I-4 This is true in a statistical sense only; as described in Chapter III, the $-q^2$ distribution in neutrino interactions is linear in the neutrino energy (see reference [I-2]), whereas charged lepton scattering has a $1/q^4$ distribution.

CHAPTER II

EXPERIMENTAL ARRANGEMENT

Data Collection

The data in this study come from Experiment 546 performed at the Fermi National Accelerator Laboratory by research groups from the University of California at Berkeley, the Lawrence-Berkeley Laboratory, FNAL, the University of Hawaii, the University of Wisconsin, and the University of Washington. The experiment employed the FNAL quadrupole-triplet neutrino beam and the 15-foot bubble chamber with the External Muon Identifier, which was expanded and upgraded by this collaboration for this work.

The neutrino beam was produced as follows. Protons accelerated in the Main Ring to a momentum of 400 GeV/c were extracted over a 'spill' period of approximately 2-3 milliseconds and directed at a one meter long aluminum oxide target. Charged secondary particles emerging from this target (mostly pions and kaons) are focussed by three successive quadrupole magnets, whose currents are set to optimize the focussing of 200 GeV/c secondaries. These secondaries then travel down a 400 meter long evacuated 'decay pipe', permitting many to decay. Between this decay pipe and the detector systems is an earthen berm, approximately one kilometer in length, which effectively filters everything that comes from the decay pipe except neutrinos

and antineutrinos. The neutrinos, mainly muon type neutrinos from the decays $\pi^+ \rightarrow \mu^+\nu$ and $K^+ \rightarrow \mu^+\nu$ (and a smaller amount of muon antineutrinos from the charge conjugate decays) then pass through the detector systems, where their interactions can be observed. Figure 2-1 illustrates the general layout of the Main Ring and neutrino beam. The spectrum of muon neutrinos and antineutrinos expected from this configuration is illustrated in figure 2-2 [II-1]. During the data collection period of this experiment (20 October, 1977 through 1 February, 1978), an average of 10^{13} protons per accelerator cycle (and thus, per bubble chamber picture) were directed onto the target, giving a total of $3.48 * 10^{18}$ protons for the entire experiment.

The detector system used was the FNAL Hybrid 15-foot Bubble Chamber/Two Plane EMI, depicted in figure 2-3. The bubble chamber was filled with a 47 percent (atomic) neon in hydrogen mixture, yielding a 55cm. radiation length and a typical pion absorption length of 1.9 m. The superconducting magnet at the bubble chamber's equator was operated with a 5000 ampere current that yields a 30 kilogauss field at the bubble chamber center. This achieves a curvature in the trajectory of charged particles which traverse the chamber, with a radius of curvature proportional to the particle's momentum (radius of 1 meter = 1 GeV/c). Three, and sometimes four, cameras with associated flash tube systems were operated to permit different perspectives of the events to be recorded and allow for subsequent three

FIGURE 2-1

Experimental Apparatus; Main Ring, Neutrino Beam Line, 15-foot Bubble Chamber/2 Plane EMI

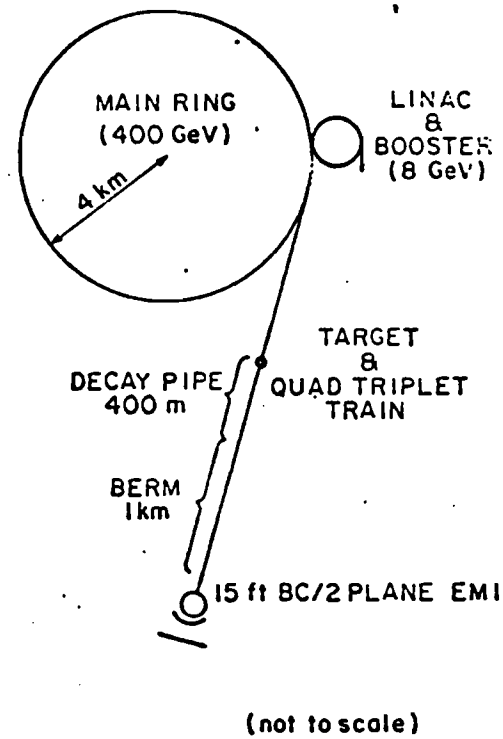

FIGURE 2-2

Neutrino energy spectrum for the Quadrapole Triplet beam [II-1]

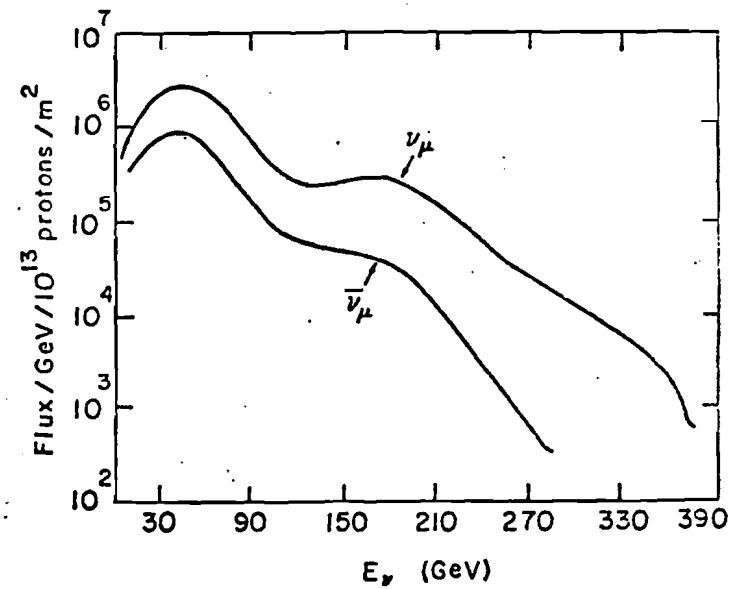

FIGURE 2-3

15-foot Bubble Chamber/2 Plane EMI

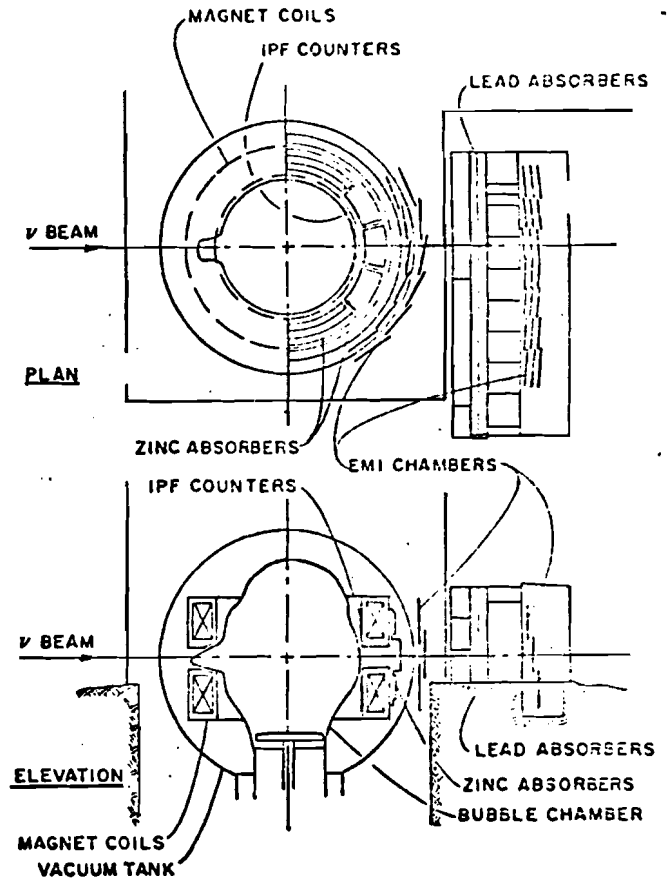

dimensional reconstruction. A total of 350,000 sets of pictures are taken, with over 326,000 accompanied by EMI data to form the data sample from which the subsequent analysis proceeded.

Lepton number conservation requires that there be the same net lepton content after an interaction as before. For an incident (muon) neutrino beam, the final state lepton can either be a neutrino again which would be virtually impossible to detect) or a negative muon. Detecting this muon permits the identification of these 'charged current' events with a concomitant understanding of the dynamics of the scattering, at least for the leptons involved. (If no muon is detected, then either the event represents 'neutral current' scattering, where the outgoing lepton, a neutrino, has the same charge as the incident lepton, or a charged current event in which the muon detection apparatus and analysis is inefficient.) The outgoing muon will identify itself by a smooth trajectory through the bubble chamber, with no large deflections indicative of hadronic scattering. Unfortunately, the bubble chamber is small enough so that it is not unusual for a hadron to exit the chamber without identifying itself as a hadron, thereby mimicking a muon. However, only the muon will traverse the several interaction lengths of lead, concrete, etc. that separate the bubble chamber and the first and then second planes of multiwire proportional chambers that constitute

the EMI (see figure 2-4) [II-2,3]. Muons are thus identifiable by extrapolating the trajectories of all smooth, leaving tracks to both EMI planes and comparing the extrapolated positions with the actual hit positions in the appropriate chambers. Details of the EMI, and discussion of the actual muon selection criteria are given in Appendix A.

Data Reduction

The primary interest in this experiment was analysis of the charged current neutrino interactions, those in which a muon is produced. For this reason, the initial scan of the film was to find all neutral-induced interactions in which there is a muon candidate, i.e. at least one long, smooth, leaving track. All such tracks were measured, reconstructed (using the geometry programs TVGP or HYDRA), and extrapolated to the two EMI planes. The relevant EMI data were unpacked and reconstructed, and those muon tracks identified according to criteria requiring two nearly simultaneous hits (one per plane) that were spatially near the extrapolated positions. Approximately 12,000 neutrino, and 2000 antineutrino events were so identified. Efficiencies and backgrounds for this identification procedure are thoroughly discussed in references [II-3,4,5].

Full measurements of the neutrino events proceed much like those to identify the muons, except that the full measurements are of all primary vertex tracks and many of the tracks from neutral induced secondary vertices. More

FIGURE 2-4

Schematic of the EMI with associated data collection electronics

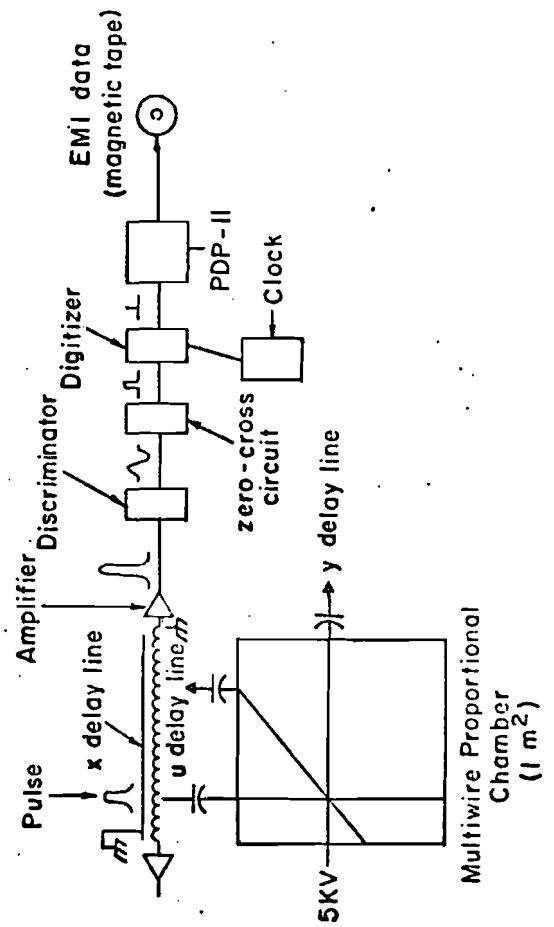

restrictive criteria were applied to the selection of the events for full measurements, as described in Appendix B. This appendix describes also the measuring rules employed, and the kinematic cuts imposed on those measured events that were used for the analysis.

NOTES TO CHAPTER II

II-1 R. Stefanski, private communication.

II-2 R. J. Cence, et al., Nucl. Inst. and Meth. 136, 245 (1976)

II-3 S. Parker, J. Marriner, and J. Orthel, IEEE Transactions on Nuclear Science 25, 1 (1978)

II-4 H. C. Ballagh, et al., Phys. Rev. D21, 569 (1980)

II-5 J. Orthel, Ph.D. Thesis, LBL-10035

CHAPTER III

THEORY

We intend to study the hadronic final state that results from (charged current) neutrino-nucleus scattering, and so we will first discuss some of the relevant theoretical topics. In that the quark-parton model governs the language, if not the mood, of the current views of hadronic processes, we will find it convenient to phrase our discussions in this terminology [III-1].

Charged Current Neutrino-Nucleon Scattering

The standard quark-parton model description of deep inelastic lepton-nucleon scattering is depicted in figure 3-1. For charged current neutrino scattering, the incident neutrino, with four-momentum k, interacts with a quark within the nucleon. The scatter results in a charged lepton, (in this study, a muon) with four-momentum k'. The momentum transferred to the quark, $q = k - k'$, has a corresponding square q^2. According to the standard view of weak interactions [III-2,3], the momentum is transferred via the exchange of an intermediate vector boson. This boson, of momentum q and virtual mass q^2 ($q^2 < 0$), will only exist over times and distances corresponding to the inverse of its mass - so the magnitude of q^2 measures the deepness of the scatter. That is, very large (negative) q^2 scatters correspond to only a small volume within the target nucleon

FIGURE 3-1

Figurative depiction of the scattering process:

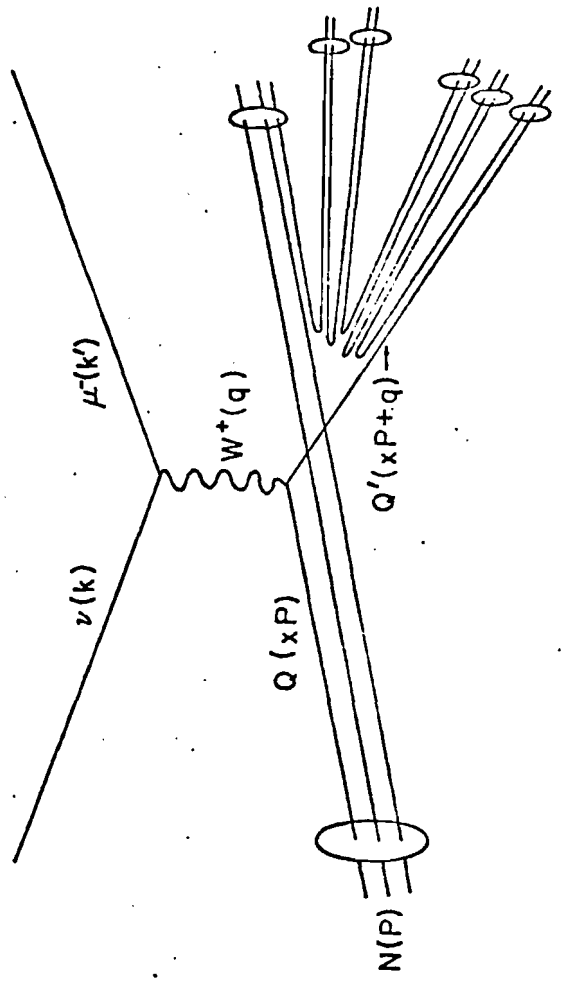

The axis of motion between the quark and the nucleon remnant is the only preferred direction in this system, and provides for a natural decomposition into longitudinal and transverse components for the individual hadrons' momenta. If we ignore the transverse components for the time being, we can describe exclusive hadron production, i.e. the process $\nu N \to \mu^- hx$, by [III-5]

$$\frac{d^3\sigma}{dxdydz} = \frac{G^2 s}{2\pi}\left| \sum Q(x,q^2)\sum{}' D^h_{Q'}(z,q^2) + (1-y)^2 \sum \bar{Q}(x,q^2)\sum{}' D^h_{\bar{Q}'}(z,q^2)\right. \qquad (3\text{-}2)$$

We introduce the fragmentation functions, $D^h_Q(z,q^2)$, as analogs of the quark distribution functions $Q(x,q^2)$. They represent the probability of a quark of flavor Q fragmenting into a hadron of type h with a fraction z of the quark's momentum. We indicate the possible q^2 dependence by analogy to the distribution functions; the details of the hadronic system from lepton-nucleon scattering may depend on the distances over which the scatter takes place. In the above, the sums over flavors Q include only those with weak hypercharge of -1/2; similarly, the sums over flavor Q' must be a hypercharge +1/2 quark, and must be weighted by the relative probability of the Q to Q' transition. For example, the sum over Q' in a four flavor model when Q indicates a 'down' quark as target will include the fragmentation function for an 'up' quark, weighted by the square of the

cosine of the Cabibbo angle, and the fragmentation function for the 'charm' quark, weighted by the square of the sine of the Cabibbo angle. [III-6])

To the extent that transverse and longitudinal momentum do factorize, transverse momentum can be included in equation 3-2 simply by multiplying the right hand side by the distribution function for transverse momentum. This distribution is outside the quark-parton model. Phenomenologically, we find it well represented by an exponential [III-7], i.e.

$$\frac{d\sigma}{dp_t^2} \propto e^{-bm_t} \qquad (3\text{-}3)$$

where $m_t = \sqrt{p_t^2 + m^2}$ is the 'transverse mass', and the parameter b approximately equal to 6/(GeV/c). There are two important aspects to this parameterization: one is that it describes transverse momentum in magnitude, not in terms of dimensionless variables, and the other is that there is no indicated dependence on q^2, W or other variable. This latter characteristic is significant in that it is really a non-scaling phenomenon (that is, changing one's measurement units changes the values for this quantity, in contrast to, for example, the fragmentation variable). It indicates that the source of transverse momentum is related to some characteristic of hadrons themselves, and not the process by which they are formed.

We have been considering only the fragmentation of the struck quark so far, and ignoring the nucleon fragment.

being sampled, whereas values of q^2 nearer to zero correspond to scatters in which larger structures within the target participate.

The leptons' behavior is of interest to us only to tell us how much energy and momentum is delivered to the nucleon (q), and the depth of the scatter (q^2). We now concentrate on the target itself. The quark that is struck has both the momentum given it and that which it had before the collision. Unfortunately, we do not know the distribution in momentum of the constituents of a nucleon, so we must rely on the quark-parton model to approximate the struck quark's momentum. This approximation gives the quark a momentum xP, where P is the nucleon's four-momentum, and x is a scalar that measures that fraction of the nucleon's momentum along the axis of the lepton-nucleon scatter contained by that quark. The neglect of quark momentum components transverse to this axis is permitted only if we view the scatter from a reference frame in which the nucleon's momentum along this axis is tremendously large (large enough so that the ratio of transverse to longitudinal momentum of a quark is truly negligible). With this approximation, we can write the cross section for neutrino-nucleon charged current scattering as [III-4]

$$\frac{d^2\sigma}{dxdy} = \frac{G^2 s}{2\pi}\left[\sum Q(x,q^2) + (1-y)^2 \sum \bar{Q}(x,q^2)\right]. \qquad (3\text{-}1)$$

Here $s = (k+P)^2$ is the total invariant energy (squared),

$y = (q\cdot P)/(k\cdot P)$ is the inelasticity of the scatter, and G the Fermi constant measuring the strength of the weak interaction. The functions $Q(x, q^2)$ and $\bar{Q}(x, q^2)$ are the distribution functions for the various flavors of quarks in the nucleon. That is, Q represents the probability of finding a quark with momentum fraction x within a nucleon, using a probe of virtual mass q^2. The sums are over all flavors of quarks or antiquarks that have a weak hypercharge of -1/2, the only ones that participate in charged current processes with neutrinos. (The factor $(1-y)^2$ that multiplies the antiquark distributions arises from conservation of angular momentum, in that only helicity -1 (+1) fermions (antifermions) participate in charged current weak processes, which results in a spin 1 neutrino-antiquark state. The resulting muon and antiquark have a $(1 + \cos\theta)^2$ distribution, which in the limit of high neutrino energies is approximated by $(1-y)^2$.)

Hadronic Final State

We now focus our attention on the evolution of the final hadronic state that results from this scattering process. Viewing the hadronic system from its center of mass reference frame, we have a quark and the remnants of the nucleon rapidly separating from each other. The observed final state, however, consists of several hadrons with various momenta, so our interest is in learning the details of how the quark-nucleon remnant state becomes the collection of hadrons observed.

which may be motivated by prejudices about quark-parton dynamics and attempt to explain the principles underlying the data, this model uses general characteristics of the data as input, and only attempts to illustrate the effects of well known physical concepts on the final distributions. Especially as it will be employed in this study, the LPS model is useful to illustrate what aspects of the various distributions are not significant. For example, as employed so far, the quark-parton model indicates that there is no connection between the longitudinal momentum fraction of a given hadron and its transverse momentum. However, in that a hadron whose longitudinal fraction is nearly equal to one virtually defines the total hadronic momentum by itself, its transverse momentum must certainly be much smaller than average. The LPS model, embedded in a Monte Carlo, will illustrate a smooth trend in the average transverse momentum of large momentum fraction hadrons toward zero p_t when the fraction approaches one, thereby indicating that this aspect of the data is purely kinematic. Other possible correlations not resultant from those processes reproduced by the LPS model will then be evident as deviations from the model's predictions.

Field and Feynman Model

In contrast to the LPS model, the model of Field and Feynmann (FF) makes some rather specific prescriptions for the various distributions involved in hadronization

[III-10, 11, 12]. Not only are algebraic forms given to the several distributions, but this model also includes the effects of the production and subsequent decay of meson resonances, an important fact to consider when one compares a model to real data. It is partially phenomenological in that several distributions are given as functions of parameters that are adjusted to fit available data. As for the LPS model, a Monte Carlo simulation based on the FF model has been performed, and will be compared to the data. For this model, the objective of the comparison will be to see how accurately the model agrees with our data.

The basic concept of this model is that the ejected quark fragments into hadrons by the creation of a quark-antiquark pair. This pair is given relative transverse momentum corresponding to a gaussian distribution. The original quark and the newly formed antiquark are combining to form one of the various vector or pseudoscalar mesons that have that (valence) quark content. This newly created meson is given a fraction of the original quark's longitudinal momentum, and the transverse momentum which is the sum of the transverse momentum of the quark and antiquark that constitute it. The leftover quark, with its transverse momentum and the remaining longitudinal momentum, now fragments in the same fashion. This procedure is iterated until the remaining energy is too small to form any new mesons. The phenomenological aspects are the functional form of the

However, when we view the hadronic system from its center of mass reference frame, we note very strong symmetry between the quark and the nucleon remnant. Besides having equal and opposite momenta, the two will have complementary quantum numbers, in that the sum of the two will be the quantum numbers of the target nucleon plus the weak boson. Thus, we need to consider the fragmentation of the diquark system as well as that of the quark. With no reason to presume differently, we anticipate the same description of the diquark as for the quark in fragmenting, other than that the functional forms (that of the fragmentation function), will reflect the distinctions of the quantum numbers. We shall be interested in comparing these two systems to see just how similar their characteristics are.

Models of Hadronization

We will now briefly consider a few models that attempt to describe the evolution of the separating quark and diquark into the observed final state.

Longitudinal Phase Space

This model is really only a minor extension of the quark-parton model, in that it only provides exact forms for the distributions that we presented above. The main virtue of this model is that it inputs distributions that reproduce the observed characteristics of hadronic systems in a very general way, and is therefore, dominated largely by

conservation laws, e.g. momentum, energy, charge and baryon number. Because the general structure of the various distributions are dominated by the constraints of phase space and conservation laws, this model then permits us to see what aspects of our data are due to such well known physics, and, by extension, which aspects are due to the actual dynamics of the hadronic system development.

The use of the term 'longitudinal phase space' for this model refers to the fact that the only real degree of freedom in producing hadrons in the model is in the selection of the longitudinal momentum component. That is, momenta for the hadrons are chosen such that the rapidities are uniformly distributed between the allowed kinematic limits. (Rapidity is defined as the arcsinh(p/E), where p and E are the longitudinal momentum and the energy of the individual particle.) Transverse momentum is, of course, modeled; it is selected according to an exponential distribution in the transverse mass, with a slope parameter corresponding to known p_t distributions from previous results. However, such transverse momenta are so small that they are rarely constrained by phase space considerations. For the purposes of comparison with this analysis, a Monte Carlo simulation based on a longitudinal phase space model has been performed. Details of this simulation can be found in Appendix C [III-8,9].

Before leaving this topic, we would like to emphasize the philosophical aspect of this model. Unlike other models,

by QCD at present ("non-perturbative QCD") are those that scale, whereas the non-scaling phenomena are within the realm of perturbation theory applied to QCD. One then 'calculates'a process as having a non-perturbative part (that one obtains from the quark-parton model applied in other kinematic regions), and adds as many orders of QCD 'corrections' as one wishes to include. The kinematical variables that one usually considers for identifying the regions of validity are measured by q^2 and/or W, so variations in hadronic distributions with these variables may indicate the onset of QCD processes.

NOTES TO CHAPTER III

III-1 Many references exist that discuss aspects of the quark-parton model; some of the germinal ones are:
R. P. Feynmann, Photon-Hadron Interactions, Benjamin Press (1972)
J. D. Bjorken, Lectures given at the International Summer Institute in Theoretical Physics, DESY, Hamburg (1975); SLAC-PUB-1957 (1976)
Y. Ne'eman, Nucl. Phys. 25, 222 (1961)
M. Gell-Mann, Phys. Rev. 125, 1067 (1962)
M. Gell-Mann, Phys. Lett. 8, 214 (1964)
For discussion of the quark-parton model from the point of view of neutrino scattering, see D. H. Perkins, Lectures given at the Summer Institute on Particle Physics, SLAC (1978) SLAC report #215.

III-2 S. Weinberg, Phys. Rev. Lett. 19, 1264 (1967)

III-3 A. Salam in Elementary Particle Theory, ed. by N. Svartholm, Almquist and Wicksell (1969) pg. 367

III-4 See, for example, E. D. Commins, Weak Interactions, McGraw-Hill (1973) and also A. DeRujula, et al., Rev. Mod. Phys. 46, 391 (1974)

III-5 D. H. Perkins, Lectures given at the Summer Institute on Particle Physics SLAC (1978) SLAC report #215

III-6 N. Cabibbo, Phys. Rev. Lett. 10, 531 (1963)

III-7 N. Schmitz, Proceedings of the 1979 International Symposium and Lepton and Photon Interactions at High Energies, Batavia (1979) pg. 359

III-8 The algorithms and procedures for this Monte Carlo program are similar to that described in the appendix in J. Bell, et al., Phys. Rev. D19, 1 (1979)

III-9 G. Swider, University of Washington Internal Note VTL-PHY-76 (1980)

III-10 R. D. Field, R. P. Feynmann, Phys. Rev. D15, 2590 (1977)

III-11 R. P. Feynmann, R. D. Field, G. C. Fox, Nucl. Phys. B128, 1 (1979)

longitudinal momentum sharing, the width of the transverse momentum gaussian, and the probabilities of forming the several meson types.

There is one major shortcoming in comparison of the FF model with our data. This model, as presented by its authors, deals exclusively with the fragmentation of a single quark. As a result, deep inelastic lepton-nucleon scattering can be modeled only in terms of the quark jet, in the laboratory reference frame, with no equal status for the diquark jet. Baryon production is not considered, either as the final hadron in a quark fragmentation function, or as the product of diquark fragmentation. As a result, comparisons of the two jets are of little relevance within the context of this model.

Quantum Chromodynamics

It is rather inappropriate to label quantum chromodynamics, QCD, as a model of hadronic processes, because QCD is much more than a phenomenological model. QCD is presently the leading candidate theory for hadronic physics [III-13]. Although its calculation abilities are still somewhat restricted, it provides a framework for understanding features of hadronic interactions in at least a qualitative way.

We will not make as full use of QCD as we will of the models in this study. This is primarily because the areas where QCD is best able to calculate are usually the 'hard'

processes, i.e. those in which the gluon (the analog to QED's photon) is very virtual [III-14]. These processes, although often quite well identified, are much less likely to occur than the 'soft' processes. That is, the majority of hadrons that will contribute to the various distributions probably arose from a process that should be within the domain of QCD, but is not calculable at present. An attempt to model the calculable 'hard' processes must be blended with a non-QCD model that will produce the more common 'soft' processes, and also dominate the calculation. (One can, of course, search for specific processes and patterns in the data which qualitatively distinguishes the QCD-related aspect of the modeling, but such a specific effort is not a part of this study.)

Much of the purpose of mentioning QCD in this study is the interest in using it as an extension of the quark-parton model [III-15, 16]. An integral aspect of QCD's limited calculational ability is that the techniques of perturbation theory are not available until one considers kinematical regimes where QCD's coupling constant (which measures the strength of the fundamental interaction) is small. Moreover, the scaling hypothesis and the quark-parton model have been quite successful in describing hadronic processes that do not change significantly with different incident energies, momentum transfers, etc. This suggests the following hypothesis; characteristics of hadronic processes not calculable

III-12 R. D. Field, R. P. Feynmann, Nucl. Phys. B136, 1 (1978)

III-13 W. Marciano, H. Pagels, Phys. Rep. 36, 137 (1978), and references contained within.

III-14 J. Ellis, Proceedings fo the 1979 International Symposium on Lepton and Photon Interactions at High Energies, Batavia (1979) pg. 412

III-15 G. Altarelli, G. Parisi, Nucl. Phys. B126, 298 (1977)

III-16 J. Ellis, Lectures given at the Summer Institute on Particle Physics, SLAC (1978), SLAC report #215

CHAPTER IV

DATA ANALYSIS AND PRESENTATION

Event Selection and Measurement

From the sample of events with identified muons, we have selected a subsample with well-identified negative muons that were in a more restricted volume within the bubble chamber. Of these 9600 events, approximately 4000 were measured completely. One thousand of these were specifically chosen for measurement because the muon had a momentum component perpendicular to the incident neutrino's direction greater than 4 GeV/c. We chose these high p-perp muon events to obtain an enriched sample of high $-q^2$ events, since, with the neglect of the muon's mass,

$$-q^2 = (p_\perp^\mu)^2/(1-y). \qquad (4\text{-}1)$$

The remaining measured events were selected in an unbiased fashion.

The specific measurement procedures are discussed in Appendix B. The objective of these measurements was to facilitate the study of the final state hadronic system. This requires careful measurement of the tracks from charged hadrons, and those from neutral-induced vertices (e.g. photon materialization, when the photon comes from neutral pion decay, or neutral strange particle decay into two charged particles). Since not all the energy from the neutral hadrons is observed, we will avoid problems with the

incomplete knowledge of the neutral hadrons and concentrate only on the charged hadrons. The measurement of the products of the neutral hadrons will still be used in determining the best estimate for the total hadronic system momentum vector.

Monte Carlo Simulation

The two models discussed earlier, the LPS model and the FF model, have been embedded into Monte Carlo programs that generate "events" in a similar format to that the data are in. This permits the results of the two models' simulations to be processed in nearly identical fashion. Thus, many of the biases that result from our measurement procedures and analysis techniques are mimicked, yielding "predictions" for the two models that are suitably modified to permit direct comparison with the data. We will make considerable use of these results in the following analysis. (The details of both of these simulations are discussed in Appendix C.)

Energy Estimation

The energy of the incident neutrino is equal to the sum of the components of the muon momentum and the total hadronic momentum in the neutrino's direction. The visible hadronic system (the charged hadrons and the measured evidence of neutral hadrons) provides a lower limit to the magnitude of the total hadronic momentum, and is generally in a different direction. Several techniques have been developed to

estimate the true value for the total hadronic momentum based on the visible momentum and the muon's momentum (especially the perpendicular component). The one we employ here scales up the visible hadronic momentum by a factor 'g', which is defined by [IV-1]

$$g = 1 + |\vec{p}_\perp^{\,\mu} + \sum \vec{p}_\perp^{\,c}| / \sum |\vec{p}_\perp^{\,c}| . \qquad (4\text{-}2)$$

Here, the sums are over all measured momenta associated with the hadronic system, either charged hadrons or neutral hadron induced secondaries. (Note that this estimation technique alters the magnitude of the momentum only.) The estimate for the neutrino energy is then the projection in the neutrino direction of the sum of the muon momentum and the estimated total hadron momentum.

The distribution of the parameter 'g' for the measured events is displayed in figure 4-1. The mean value of $\langle g \rangle = 1.17$ corresponds to one's intuition: on average, 17 percent of the hadronic energy is not observed. The tail of the distribution, events for which 'g' is rather large, indicates that for some events this procedure results in more hadronic energy inferred than measured. In order to avoid the potentially large uncertainties that may be introduced by such events, we restrict our event sample to only those events for which $g < 3.0$. The LPS simulation indicates that the events excluded by this criterion do not preferentially occupy any particular region of the distributions of neutrino energy, q^2, etc.

FIGURE 4-1

Distribution of the hadronic energy correction factor "g" for all measured charged current events.

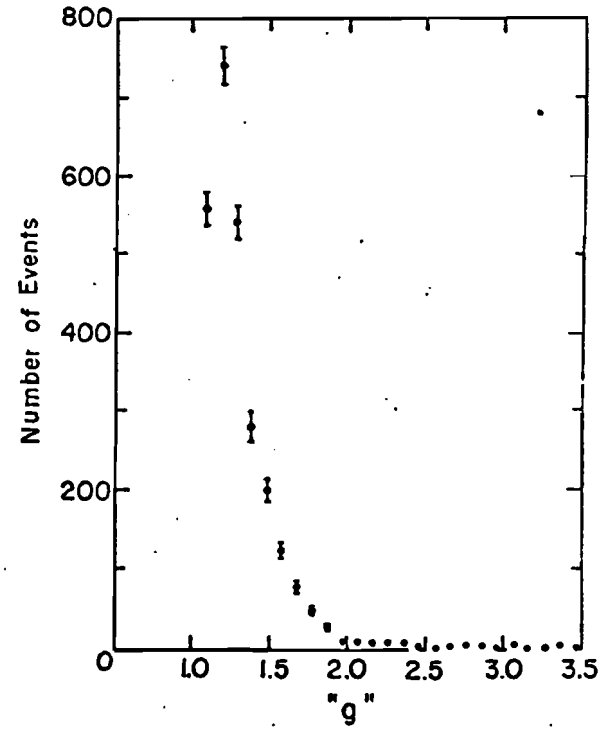

Several other criteria are imposed on the sample of measured events in order to select only that sample to be used in the analysis. Such criteria are enumerated and discussed in Appendix B. The most important ones are that restriction on the hadronic energy correction factor (mentioned above), and the requirements that the events have values $-q^2 > 2.0\ (\mathrm{GeV}/c^2)^2$ and $W > 2.0\ (\mathrm{GeV}/c^2)$. These last two restrictions are to eliminate events that will be dominated by resonance production and those events for which the available phase space is severely restricted. Such cuts are survived by 2710 events, 964 of which were from that sample selected for large perpendicular momentum muons. The (estimated) neutrino energy distribution for this, our analysis sample, is shown in figure 4-2. This can be compared in a general sense to the distribution of neutrino energies, figure 2-2, although strict comparison is pointless in that figure 4-2 contains the effects of the energy dependence of neutrino cross sections, biases due to acceptances and analysis procedures, etc. The event energy distributions from the simulations, i.e. reconstructed, estimated event energy distributions, are very similar to that from the data. One notices that another effect of the high perpendicular momentum muon preselection was to select high energy events, as the shaded region in figure 4-2 shows. The average neutrino energy for this high p-perp muon sample is 167 GeV; that of the unbiased events (which, of course,

FIGURE 4-2

Distribution of (corrected) event energy for the analysis sample. The LPS and FF model distributions (normalized to the data) are superimposed.

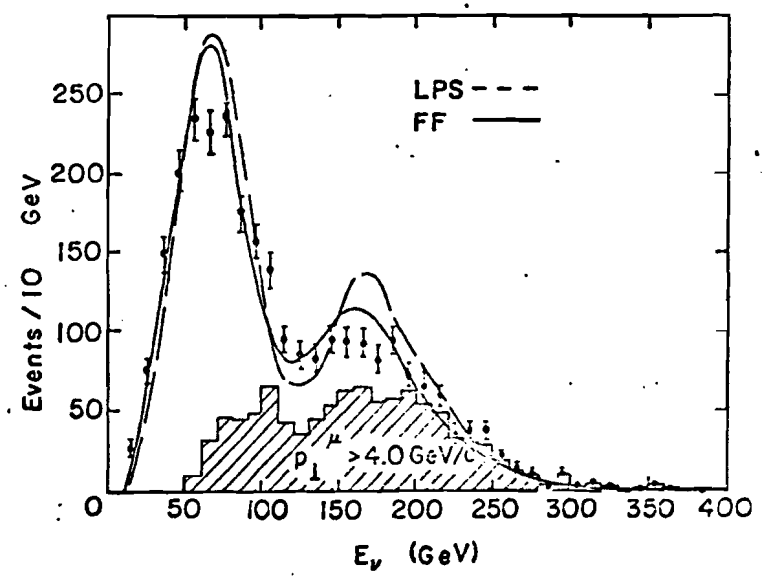

contain some events from the high p-perp muon sample) is 95 GeV, which gives an average event energy of 112 GeV for the combined sample.

With an estimate of the neutrino energy, the calculations of q^2, W^2, x, and y are straightforward. These distributions are shown in figures 4-3 through 4-7, respectively (with LPS and FF curves for comparison). The x distribution favors slightly higher values than one would expect from other experiments' data [I-2], but this is due to the selection of high $-q^2$ events from our high p-perp muon enhancement. The deviations from uniformity in y are due to the minimum muon momentum criterion (low y) and the minimum hadronic energy requirement (high y). The simulation curves, having the same mixture of high p-perp muon events and subject to similar constraints (including simulated EMI acceptance for the muon) reflect these aspects of the data.

Multiplicities

The simplest hadronic quantity to measure is the multiplicity of charged particles in an event. We plot the average multiplicities for positive, negative, and all charged hadrons, as functions of the logarithm of q^2 and W^2 in figure 4-6. These multiplicities include all charged hadrons produced by the neutrino-nucleus interaction, excluding protons when they are identified. The excess of positive hadrons over negative hadrons is of the size

FIGURE 4-3

Distribution of $Q^2 = -q^2$ for the analysis sample, with the LPS and FF model curves superimposed.

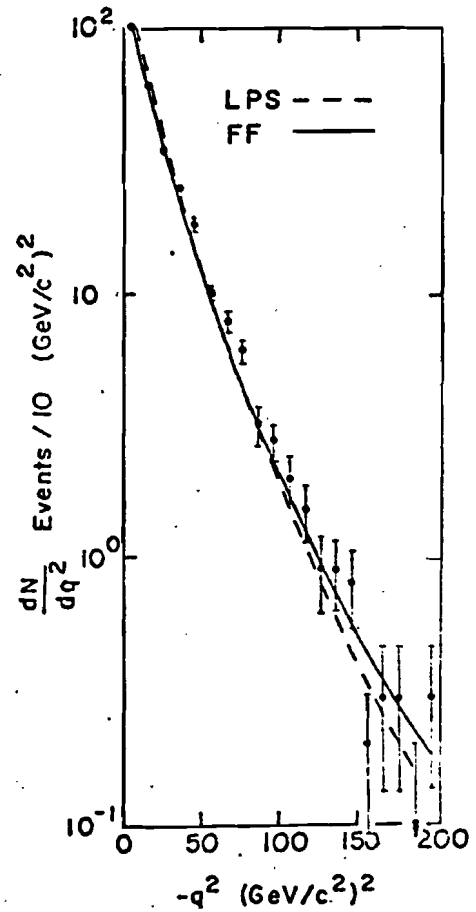

FIGURE 4-4

Distribution of W^2 for the analysis sample, with the LPS and FF model curves superimposed.

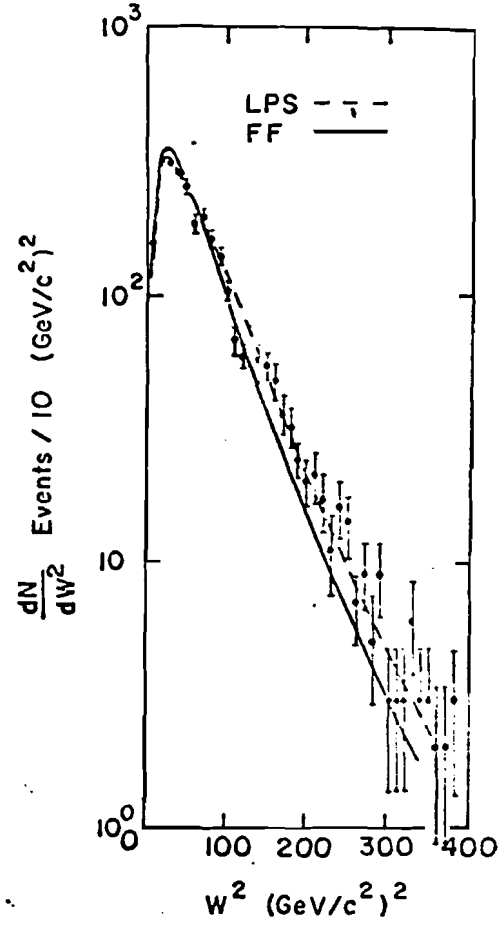

FIGURE 4-5

Distribution of x for the analysis sample, with the LPS and FF model curves superimposed.

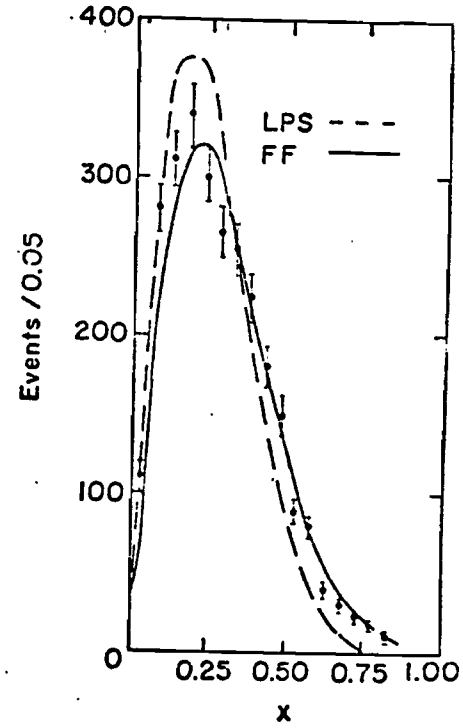

FIGURE 4-6

Distribution of y for the analysis sample, with the LPS and FF model curves superimposed.

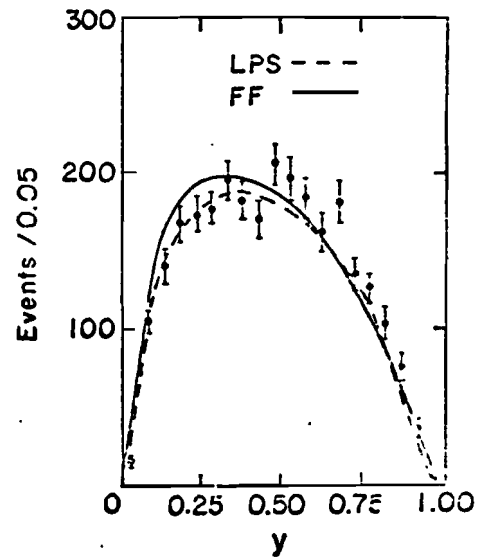

FIGURE 4-7

Multiplicities of charged hadrons, versus the logarithm of $-q^2/M^2$ (407a) and versus the logarithm of W^2/M^2 (4-7b). The curves are from the LPS model.

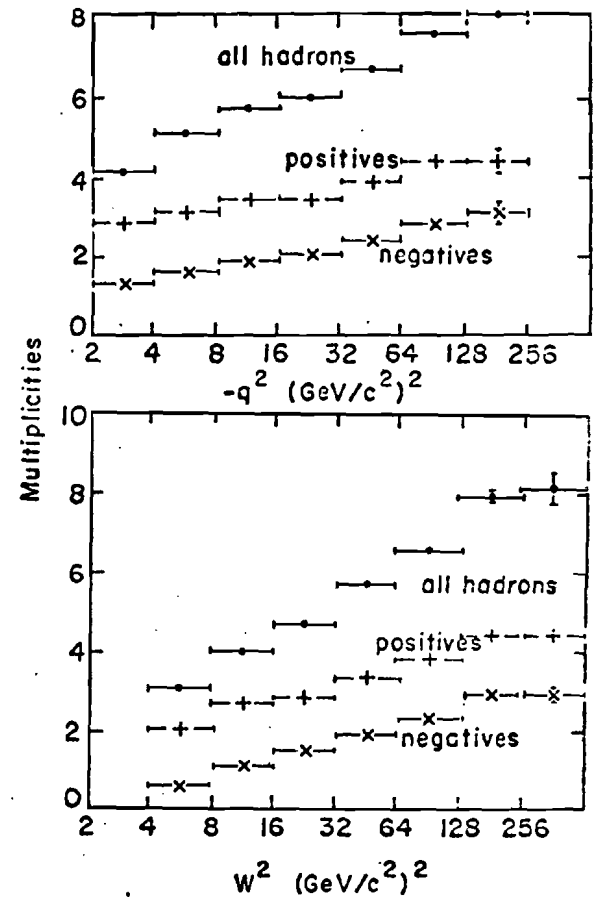

FIGURE 4-8

Distribution of $D^+(z) = 1/N\text{-}E\ dn/dz$ and $D^-(z) = 1/N\text{-}E\ dn/dz$. (Positive and negative hadrons separate). 4-8a is plotted using $z = z_+$, 4-8b for $z = z_-$. LPS and FF model curves superimposed.

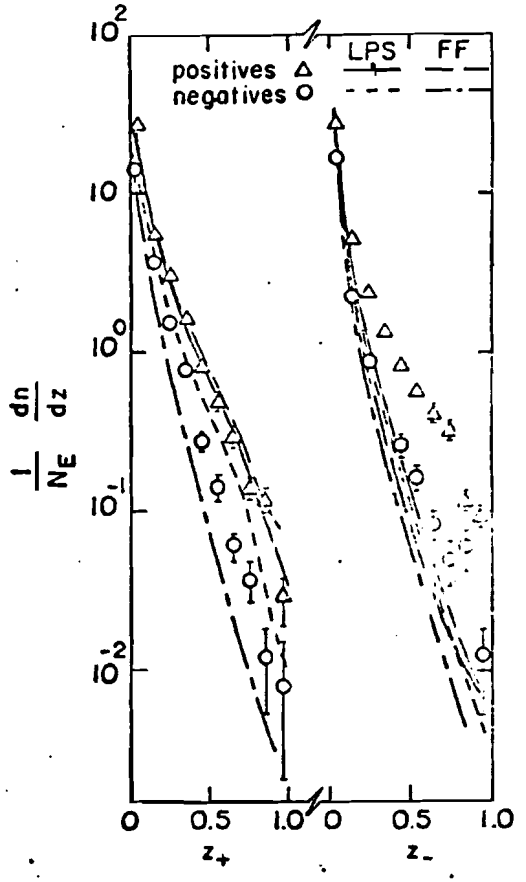

expected for a positive beam (viewing the interaction as scattering a positive weak boson with the nucleon) and a positive target. Linear fits to these data, where we use the logarithm $-q^2/M^2$ or W^2/M^2 as the abscissa (M is the nucleon mass) are quite good. The parameters of such fits, including fits for the simulation results, for comparison are listed in Table 4-1. A slight preference for linear dependence on the logarithm of W is observed; moreover, the linear fit versus the logarithm of $-q^2$ may be due to the correlation between these two variables, as the LPS data are generated according to a log(W) dependence, and yet still fit a linear dependence on $\log(-q^2)$ reasonably well. (Note that the data for all charged hadrons represent more than just the sum of the positive hadron multiplicities with the negatives. This is because there are some hadrons who interact early in their trajectory, often making charge determination inaccurate. Such hadrons are not included in either charge multiplicity, but are included in the total.)

We point out that the multiplicity of positive hadrons exceeds that of the negatives by more than one unit for all values of q^2 and W. This is due to excess protons, whose source is related to the spectator nucleons in the neon nucleus, but whose momenta are large enough to make them indistinguishable from positive pions or kaons. This phenomenon is typical for neon-filled bubble chamber experiments [IV-2, IV-3], and will present difficulties in later analysis.

TABLE 4-1

Fits of Multiplicities to Linear Equation

$$\text{mult} = a + b * \log(-q^2/M^2)$$

		a		b		χ^2/NDF
Positives	(data)	2.5	±0.3	0.86	±0.26	14.2/5
	(LPSMC)	2.7	±0.2	0.74	±0.16	2.2/5
	(FFMC)	1.6	±0.2	0.35	±0.17	71.0/5
Negatives	(data)	1.0	±0.3	0.90	±0.23	4.5/5
	(LPSMC)	2.0	±0.2	0.60	±0.16	72.7/5
	(FFMC)	0.63	±0.17	0.87	±0.16	15.6/5
All	(data)	3.9	±0.4	1.8	±0.3	10.0/5
	(LPSMC)	4.5	±.02	1.5	±0.2	2.8/5
	(FFMC)	2.0	±0.2	2.0	±0.2	15.9/5

$$\text{mult} = a + b * \log(W^2/M^2)$$

		a		b		χ^2/NDF
Positives	(data)	1.3	±0.3	1.4	±0.3	6.9/5
	(LPSMC)	1.0	±0.2	1.5	±0.2	8.2/5
	(FFMC)	0.61	±0.22	1.3	±0.2	64.6/5
Negatives	(data)	-0.23	±0.3	1.4	±0.2	7.8/5
	(LPSMC)	0.12	±0.19	1.6	±0.2	10.9/5
	(FFMC)	-0.18	±0.02	1.2	±0.2	14.5/5
All	(data)	1.1	±0.4	3.0	±0.3	8.2/5
	(DPSMC)	1.1	±0.3	3.1	±0.2	5.3/5
	(FFMC)	0.23	±0.28	2.6	±0.3	13.3/5

Momentum Distributions

We will now examine the momentum distributions of the charged hadrons. Recalling the discussions in Chapter III, we will examine the longitudinal and transverse momentum components separately, and then examine correlations between the two. For each of these subtopics, emphasis will be placed on any dependence of these distributions upon q^2, W, etc.

The separation of momentum into longitudinal and transverse components requires the definition of an axis. The direction of the struck quark provides this axis, but missing hadrons (neutrals), measurement uncertainties, etc. will make determination of this direction imprecise. We chose to use the direction of the total visible hadronic momentum as our estimate of the struck quark's direction. Studies have shown that this visible hadronic direction (VHD) is the least biased estimator [IV-4].

Longitudinal Momentum

There are several definitions of the longitudinal momentum fraction, z, which serves as an argument to the fragmentation functions. We will find it useful to employ z_+ and z_-, defined by

$$z_\pm = (e \pm p_{||})/(E \pm P_{||}) \qquad (4\text{-}3)$$

where e, $p_{||}$ (E, $P_{||}$) refer to the energy and longitudinal momentum of the individual hadron (total visible hadronic

system). The advantage to z_+ and z_- is that, as the ratios of the light-cone momenta [IV-5], they are invariant under Lorentz boosts along the longitudinal direction, which means that they have the same form no matter which frame they are evaluated in. Choosing the hadronic center of mass (CM) frame, we see that z_+ (z_-) is large for hadrons with a large momentum component in the forward (backward) direction, relative to the direction of the struck quark. Since there is a symmetry in the hadronic CM frame between the outgoing quark and the nucleon remnant that has opposite momentum, we can use z_+ to parameterize the quark's fragmentation, and z_- to parameterize that of the diquark system or nucleon remnant.

In figure 4-8 we display the distribution of hadrons in z_+ and z_-, separated by charge. These distributions, which we will denote D^+ and D^-, are equivalent to the sum of several fragmentation functions. These sums are over all positively charged quarks and antiquarks (because we do not know the flavor of the struck quark or antiquark), and also sums over all the same charge hadron species (because particle identification in the bubble chamber is not accurate enough to permit the separation), i.e. $D^+ = D_u^{\pi^+} + D_u^{K^+} + D_{\bar{d}}^{-+} + \ldots$

Focussing on the z_+ distributions, one sees the expected excess of positive hadrons over negatives, indicative of the fact that the outgoing quark has positive charge. The FF and LPS simulations both reproduce the positive hadron

distribution well; both are less accurate, in complementary fashion, in reproducing the negative hadron distribution. Looking at the z_- distributions, there is an apparent large discrepancy between the data and both models for the positive hadrons. This difference is due to excess protons. Since they are relatively low momentum, they will appear at high z_- values (the diquark fragment hadrons have low momentum when measured in the laboratory frame). Moreover, z_- is particularly subject to measurement errors, in that it involves the differences of quantities that are nearly equal. These two problems will prohibit us from making use of z_- in any detailed fashion.

For comparison, we present D^+ and D^- as functions of z_v in figure 4-9, where z_v is the ratio of the hadron's longitudinal momentum to the total hadronic momentum. These distributions are quite similar to those using z_+ as the argument, indicating that use of z_+ is equivalent to use of z_v or other more common fragmentation fraction definitions. Our results are in reasonable agreement with those of other experiments [IV-6, III-7].

We now look at the dependence of D^+ and D^- on q^2 and W. In figures 4-10 and 4-11 we show $D^+(z_+)$ and $D^-(z_+)$, where the data have been separated into low $-q^2$ and high $-q^2$ samples ($-q^2 = 15$ $[\mathrm{GeV}/c^2]^2$ is the separation). Whereas for each z_+ bin the low $-q^2$ and high $-q^2$ data are nearly equal, the low $-q^2$ points are consistently above those for high $-q^2$ for the

FIGURE 4-9

Distributions $D^+(z)$ and $D^-(z)$ for $z = z_{vis}$, plotted separately by charge. LPS and FF model curves superimposed.

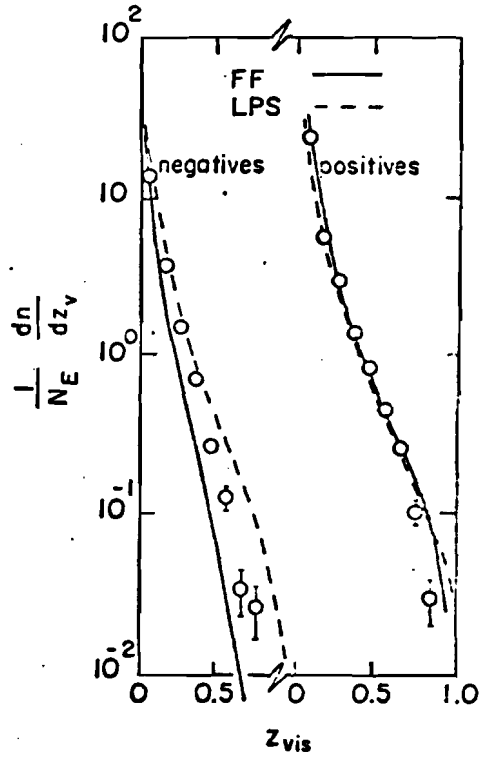

FIGURE 4-10

Distribution $D^+(z_+)$, events separated into low and high $-q^2$ (separated at 15 $(GeV/c^2)^2$). LPS and FF model curves superimposed.

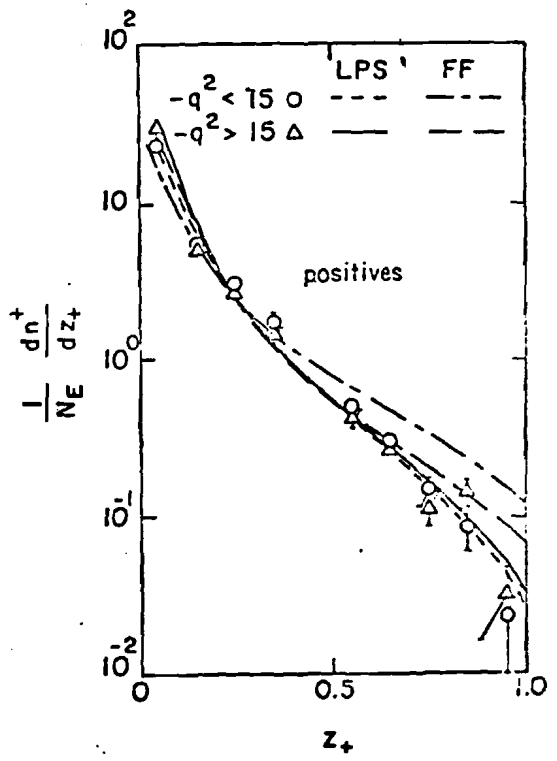

FIGURE 4-11

Distribution $D^-(z_+)$, events separated into low and high $-q^2$. LPS and FF model curves superimposed.

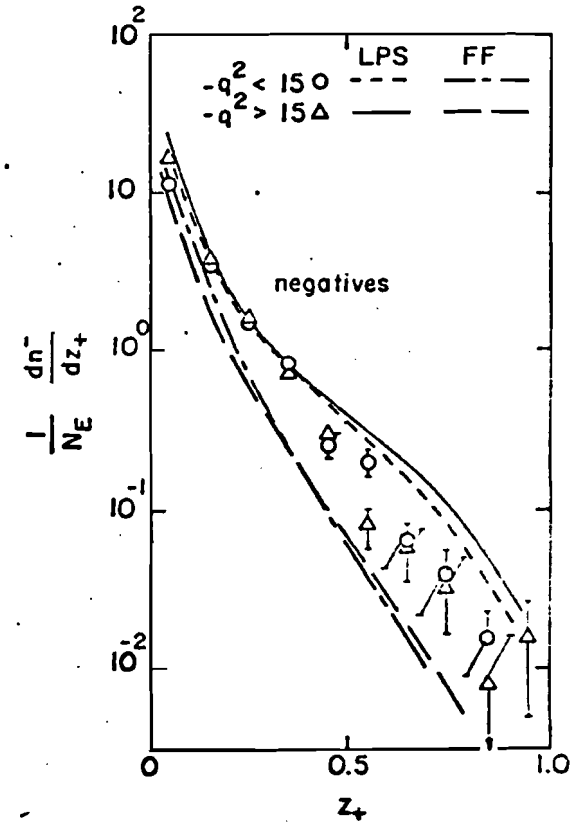

positive hadrons. For the negative hadrons, there is a slight tendency for the low $-q^2$ to exceed the high $-q^2$, but this is not statistically significant. We do the same for low and high W, dividing at $W^2 = 45\ (\mathrm{GeV}/c^2)^2$, in figures 4-12 and 4-13. As for the previous distributions, there is a tendency for the higher W^2 data to exhibit a softer fragmentation than the low W^2, but this is not a strong effect. q^2 dependent fragmentation functions have been reported in similar experiments previously [IV-7].

The LPS model fragmentation functions show virtually no q^2 or W^2 dependence, as one expects from its scaling origin. The FF model does show both a q^2 dependence, and a milder W^2 dependence; however, this model simulates neutrino scattering with antiquarks in the target nucleon, which have an x distribution very near zero, which will therefore be more in evidence in the low $-q^2$ data. That is, we anticipate that for the FF model, there is more $D_{\bar{d}}^{\pi^+}$ contribution to our D^+ distribution at low $-q^2$ than at high $-q^2$. The result is that, whereas a fragmentation function may not be q^2 dependent, the linear combination of fragmentation functions that constitute D^+ and D^- may be q^2 dependent in that the relative contributions from the fragmentation functions depend on q^2. The q^2, W^2 correlation could explain the milder W dependence.

In figures 4-14 and 4-15 we display D^+ in two q^2 samples and two W^2 samples, but now for only those events where

FIGURE 4-12

Distribution $D^+(z_+)$, events separated into low and high W^2 (separated at 45 $(GeV/c^2)^2$). LPS and FF model curves are superimposed.

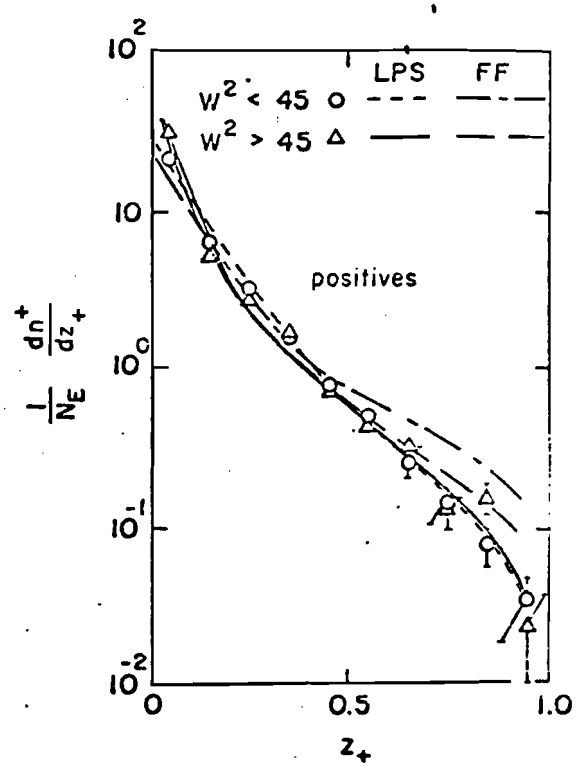

FIGURE 4-13

Distribution $D^-(z_+)$, events separated into low and high W^2. LPS and FF models superimposed.

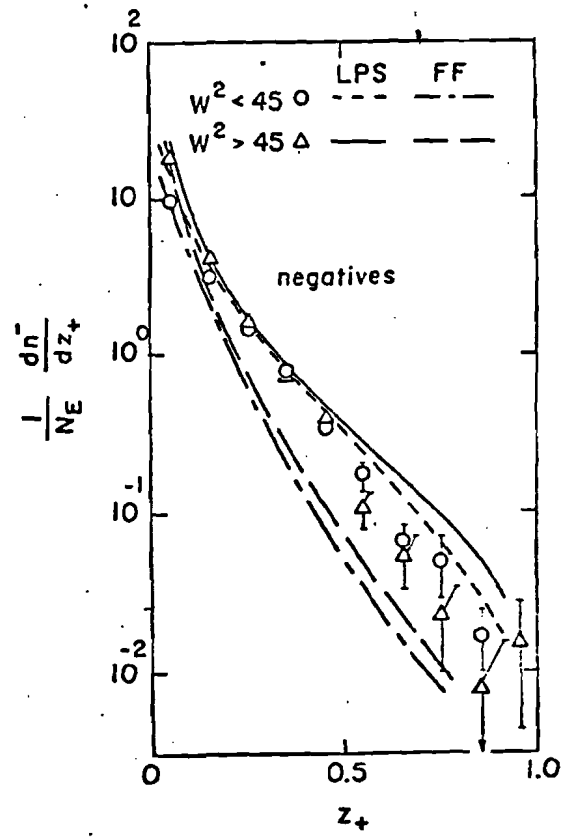

FIGURE 4-14

Distribution $D^+(z_+)$, events separated into low and high $-q^2$ (separated at 15 $(GeV/c^2)^2$), for all events with $x > 0.3$. LPS and FF model curves superimposed.

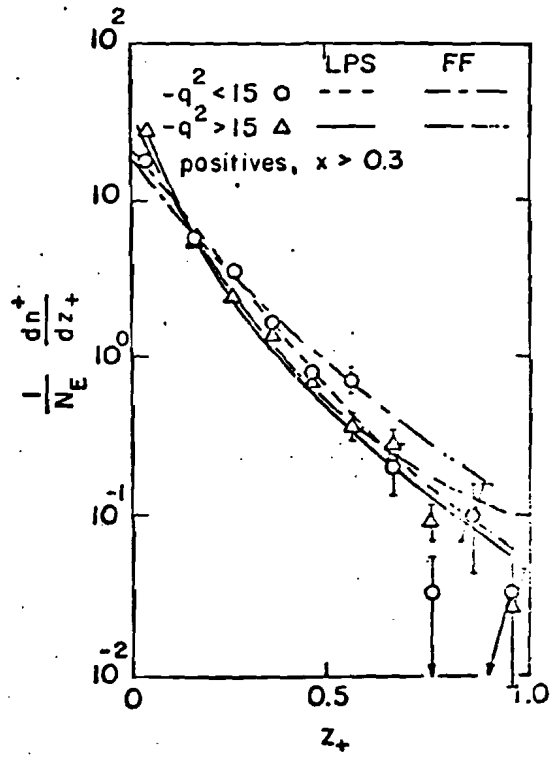

FIGURE 4-15

Distribution $D^+(z_+)$, events separated into low and high W^2 (separated at 45 $(GeV/c^2)^2$), for all events with $x > 0.3$. LPS and FF model curves superimposed.

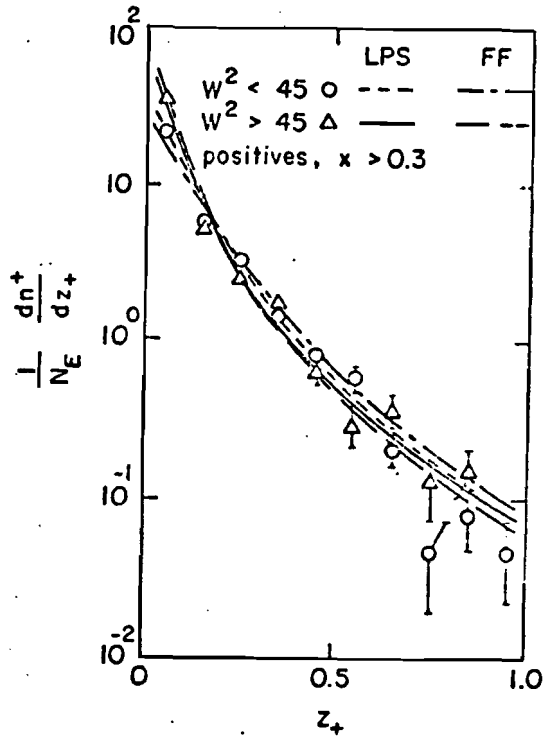

$x > 0.3$. Kinematically, this serves to separate the q^2 and W dependence, as the two variables are correlated through x. Physically, this selection enhances the data for which a valence quark in the target nucleon is struck (the 'down' to 'up' transition), since the sea quark distribution clusters near small x. Neglecting the kaon content (the number of K^0's per event, presumably similar to the number of charged K's, is 0.15), this $x > 0.3$ selection permits the approximation $D^+(z_+) = D_u^{\pi^+}(z_+)$. Again, the q^2 separated data show a reasonably consistent indication of softer fragmentation for the higher $-q^2$ data, but the effect is less pronounced than in the distribution using all x events. (The same analysis, using z_v rather than z_+, yields similar results.)

Transverse Momentum

The plane perpendicular to the VHD contains the two components of a given hadron's transverse momentum. We can systematically identify these components, because one will be perpendicular to the plane formed by the momenta of the incident neutrino and outgoing muon. In that these lepton's directions are extremely well measured, transverse momentum relative to this lepton plane (LP) is rather unbiased. Moreover, the average of p_t^2 from the lepton plane should be half that of p_t^2 from VHD, so we can check the reasonableness of using the VHD in this way.

In figure 4-16 we display the distribution of hadrons in transverse momentum (squared). Transverse momentum from

FIGURE 4-16

Distribution in transverse momentum squared for all hadrons, $1/N\text{-}E\ dn/dp_t^2$. Transverse momentum is from the VHD and the LP, with the horizontal scale expanded by a factor of two for the LP data. LPS model curves superimposed.

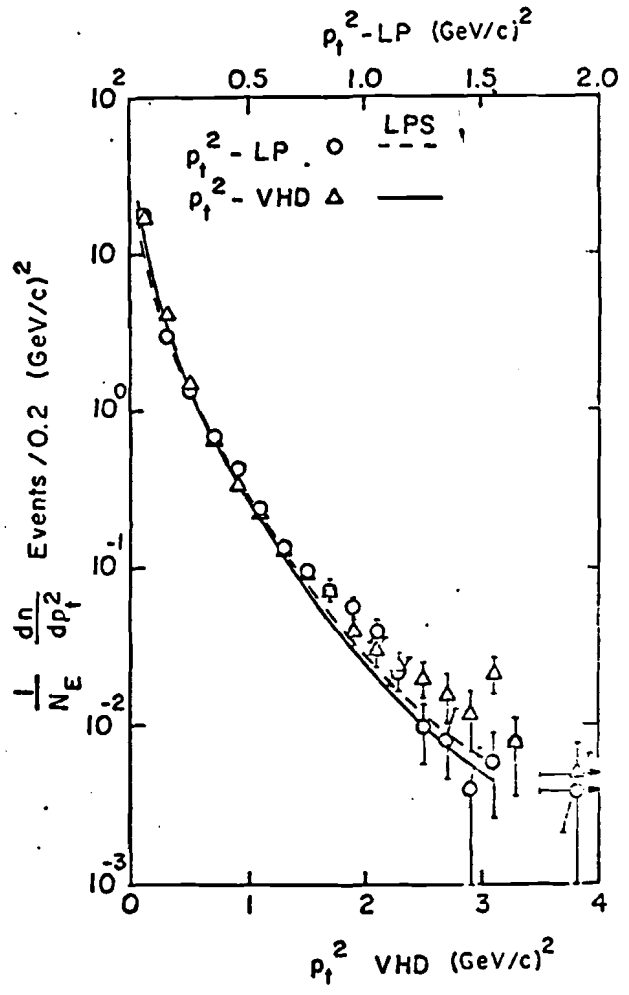

both the VHD and LP are together, with the horizontal scale for the LP data expanded by a factor of two to facilitate comparison. The agreement between the two sets of data is quite good, testifying to the reasonableness of the choice of the VHD as the longitudinal axis.

The interesting feature of figure 4-16 is the region of higher transverse momentum, approximately $p_t^2 > 1.0$ $(GeV/c)^2$ ($p_t^2 > 0.5$ for the LP data). Here we see a significant departure of the data from the LPS model prediction. The agreement with the LPS model for low transverse momentum indicates that there may be another source of transverse momentum, that gives a small number of hadrons a larger transverse momentum component. If we again split the data sample into low and high samples in $-q^2$ and W, as we do in figures 4-17 and 4-18 (VHD only), we see that this high p_t excess occurs primarily in the high $-q^2$ or high W^2 events. The low $-q^2$ and low W^2 data are well simulated by the LPS model over the full range of transverse momentum. (This high p_t with high $-q^2$ or high W^2 phenomenon is also evident using transverse momentum from the LP).

Previous neutrino and antineutrino experiments have reported no significant departure from phase space expectations in transverse momentum distributions [IV-8, IV-9, IV-10, IV-11]. However, more recent data (from neutrino experiments [IV-12]and muon experiments [IV-13, IV-14]) with incident lepton energies comparable to that of this experiment,

FIGURE 4-17

Distribution of transverse momentum squared from the VHD for all hadrons, events separated into low and high $-q^2$. LPS model curves superimposed.

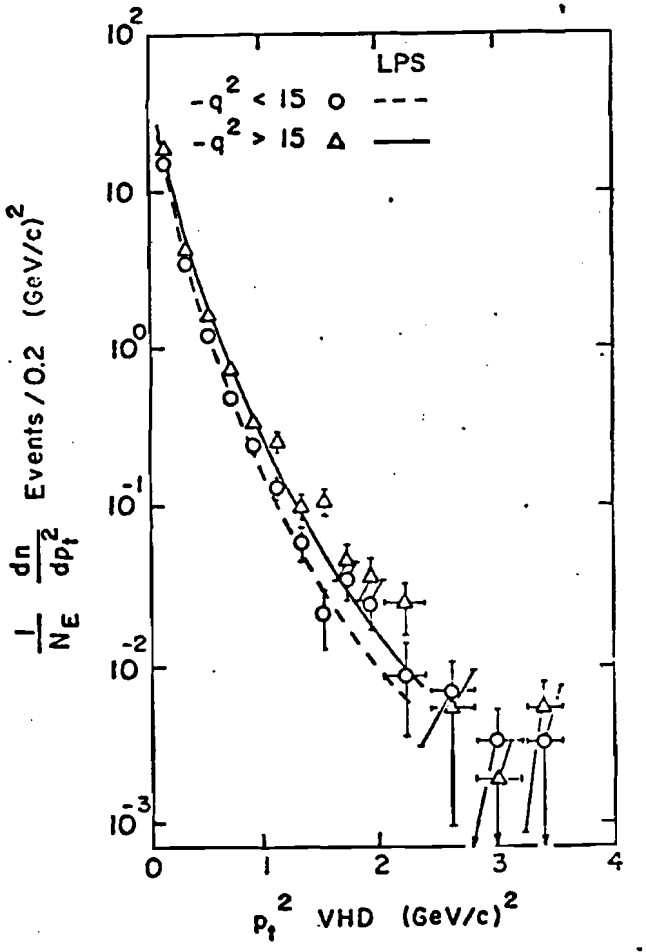

FIGURE 4-18

Distribution of transverse momentum squared from the VHD for all hadrons, events separated into low and high W^2. LPS model curves superimposed.

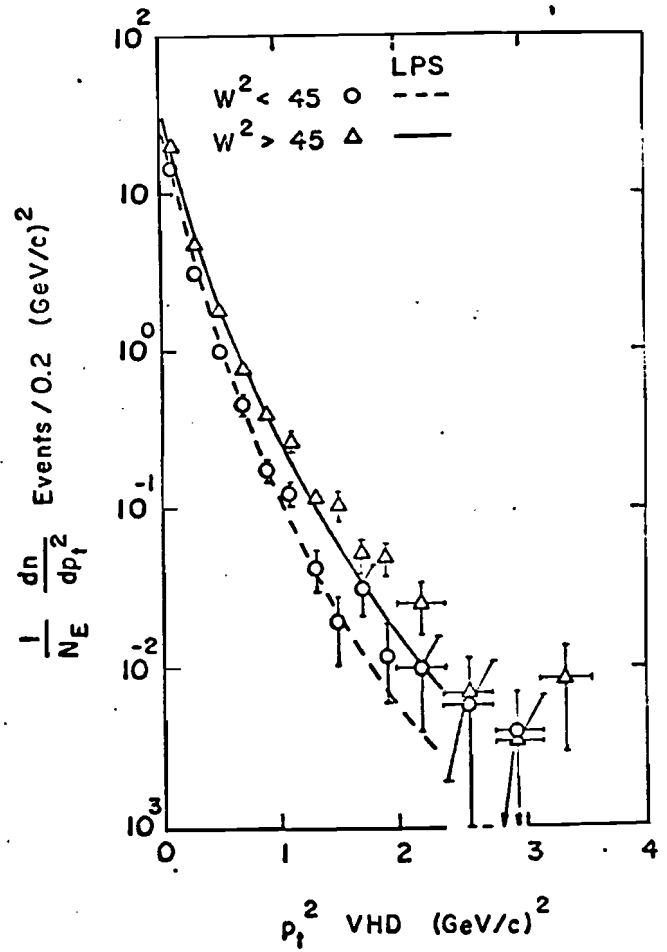

have reported rising transverse momentum corresponding to rising $-q^2$ and W^2. The earlier results that show no departure were performed with lower incident neutrino energies, corresponding to q^2 and W values where our data sees little departure from phase space.

Were we to duplicate figures 4-17 and 4-18 using smaller ranges of $-q^2$ or W^2, the statistical significance of the data would diminish quickly enough to lose the evidence of the effect. Instead, we can use average values of p_t^2, and plot these versus finer q^2 and W^2 bins. We do this in figures 4-19 and 4-20, where we see a consistently higher value of $\langle p_t^2 \rangle$ in the data than the LPS model gives, which becomes slightly more pronounced at the higher values of $-q^2$ or W^2. Unfortunately, these average values are dominated by the great majority of hadrons with only a small transverse momentum, so the effect that we are investigating, which is an enhancement in the tail of a distribution, is considerably diminished in these average value comparisons. Nevertheless, there is a statistically significant trend in such distributions.

The existence of an excess of high p_t hadrons is a bit of a delicate phenomenon because the full effect relies on only a small sample of hadrons, which could be particularly subject to measurement uncertainties, analysis procedures, etc. Investigations of several of these types of problems indicate that these hadrons are not significantly different from those in the low transverse momentum region.

FIGURE 4-19

Average p_t^2 for all hadrons, versus $-q^2$; 4-19a is for p_t^2 from the LP, and 4-19b is for p_t^2 from the VHD. LPS model curves superimposed .

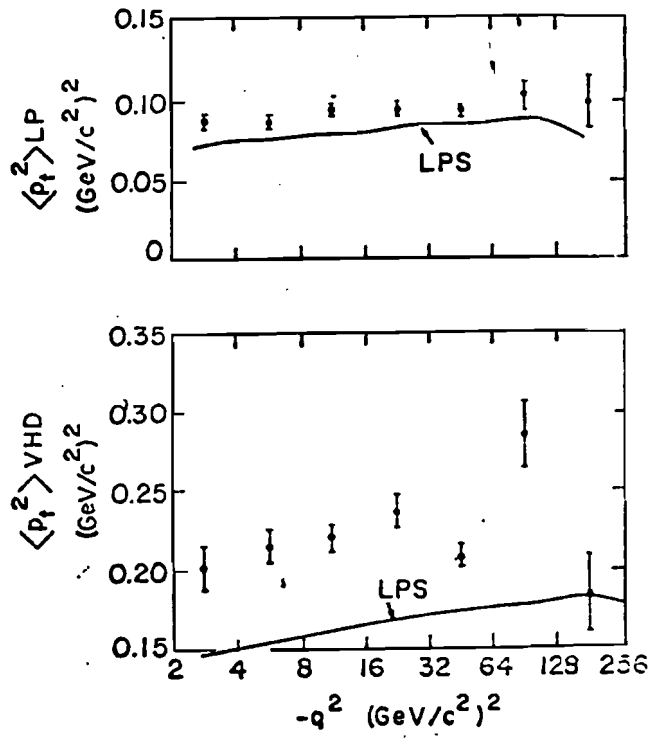

FIGURE 4-20

Average p_t^2 for all hadrons, versus W^2; 4-20a is for p_t^2 from the LP, and 4-20b is for p_t^2 from the VHD. LPS model curves superimposed.

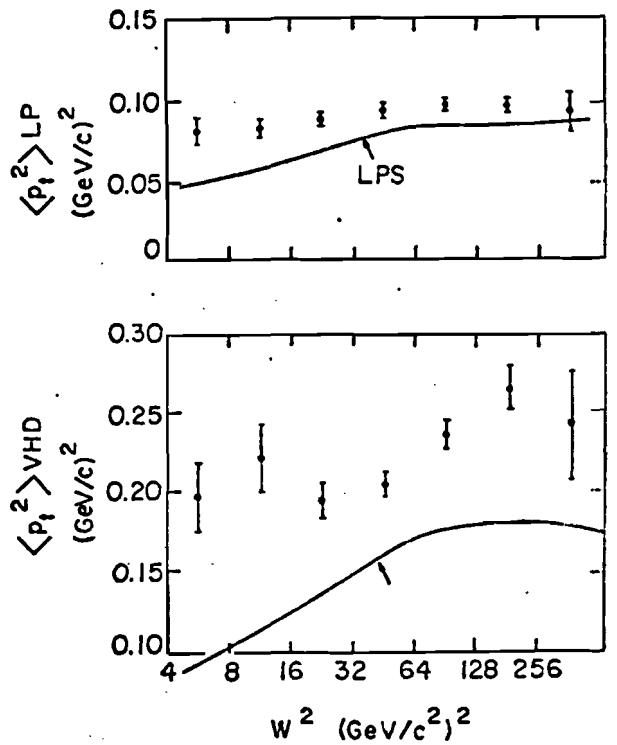

Measurement uncertainties are required to be less than 20 percent in momentum determination; whereas this affects twice as many high p_t hadrons as low p_t ones, altering this maximum uncertainty limit within reasonable values does not significantly change these results. Moreover, this momentum determination uncertainty is reproduced in the Monte Carlo simulations. The use of p_t from the LP argues against the objection that the VHD is too biased. (Use of other axes for the longitudinal direction has shown that, although all transverse momenta seem to be excessively large, there is still an excess of high p_t hadrons in the data when compared to the LPS simulations.) We conclude that any source of transverse momentum resulting from our measurement inaccuracies or analysis procedures is either well reproduced by the simulations or is only a small, negligible problem.

Correlations Between Longitudinal and Transverse Momentum

We would now like to examine the correlation between the transverse momentum and the longitudinal momentum fraction. We will do this considering the hadronic system from its CM frame, as we would like to distinguish the hadrons from the quark fragmentation from those resulting from the diquark fragmentation. The variables z_+ and z_- will serve to perform this separation; we will define the forward jet hadrons, those presumably related to the quark fragmentation, as those hadrons with $z_+ > 0.2$, and the backward jet hadrons, associated with diquark fragmentation,

as those hadrons for which $z_- > 0.2$. Although these definitions undoubtedly reject hadrons that should be included in the definition of these jets, the cut at 0.2 cleanly separates the two jets. Only a very few hadrons have z_+ and z_- values both larger than this minimum [IV-15].

We now re-examine the transverse momentum distributions, this time separating the hadrons according to which jet they are associated. Figures 4-21 (VHD) and 4-22 (LP) display the transverse momentum distributions for the two jets separately, with the distribution for all hadrons superimposed for comparison. Three characteristics are immediately obvious: the fast forward and fast backward hadrons have a much broader p_t distribution than that for all hadrons; the high p_t region of the distribution for all hadrons is populated almost exclusively by the forward jet and backward jet hadrons; and, finally, the forward jet hadrons have more of a high transverse momentum tail than the backward jet hadrons.

We now separate the events into low and high $-q^2$ and W^2 events. In figures 4-23 and 4-24 we display the distribution in transverse momentum for the forward hadrons, separated into the two $-q^2$ and two W^2 samples. In both cases we see that the low $-q^2$ or low W^2 data are consistent with the LPS model, but the high $-q^2$ and high W^2 data show a significant departure from this model in the high p_t region. (The FF model curves are also shown, but do not reproduce the data at all.) In figures 4-25 and 4-26 we display the same

FIGURE 4-21

Distribution of transverse momentum squared from the VHD for all hadrons, for forward jet hadrons ($z_+ > 0.2$), and for backward jet hadrons ($z_- > 0.2$). LPS model curves (for all hadrons) is superimposed.

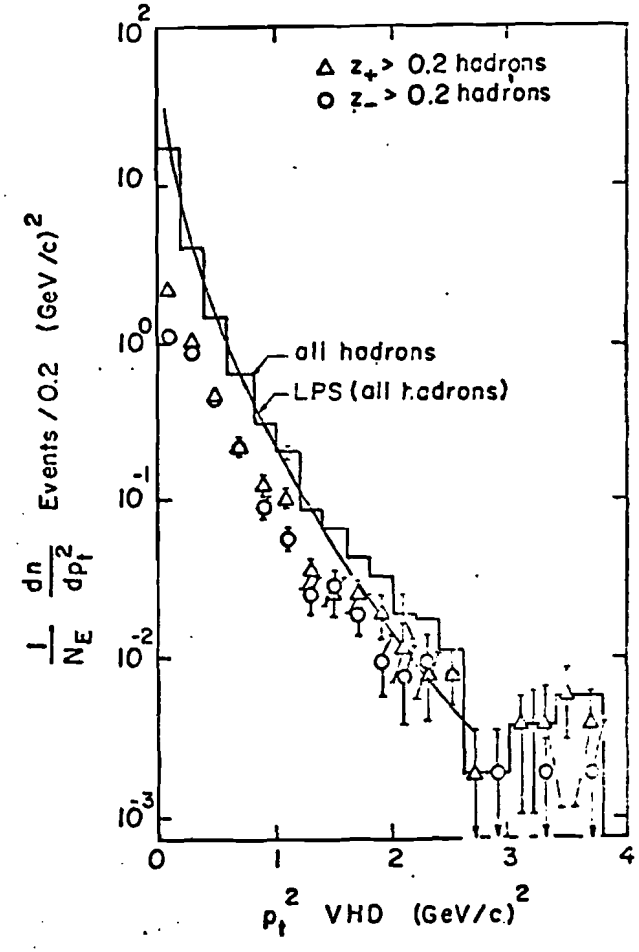

FIGURE 4-22

Distribution of transverse momentum squared from the LP for all hadrons, for forward jet hadrons, and for backward jet hadrons. LPS model curve (for all hadrons) superimposed.

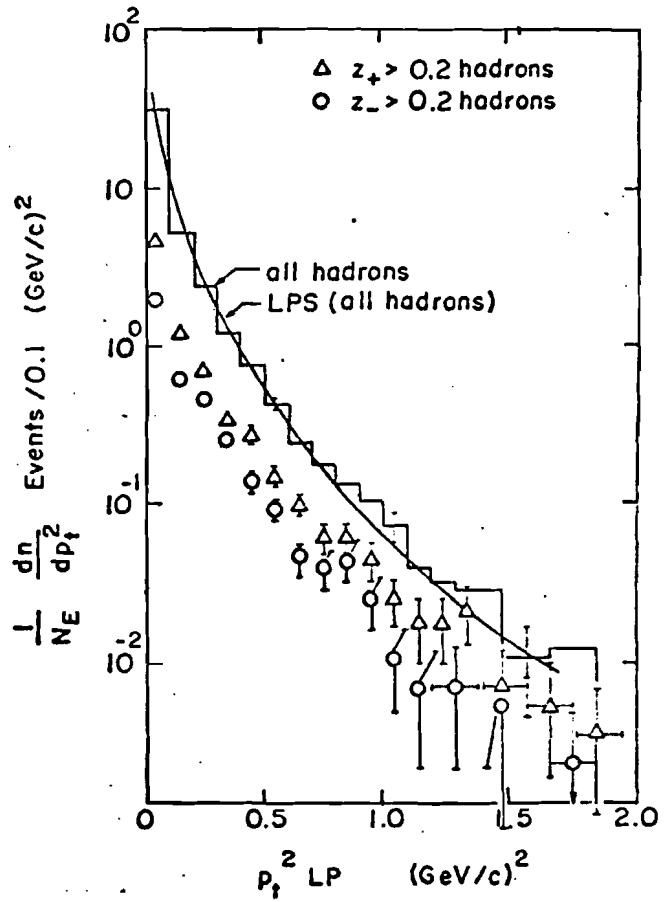

FIGURE 4-23

Distribution of transverse momentum squared from the VHD for forward jet hadrons, events separated into low and high $-q^2$. LPS and FF model curves superimposed.

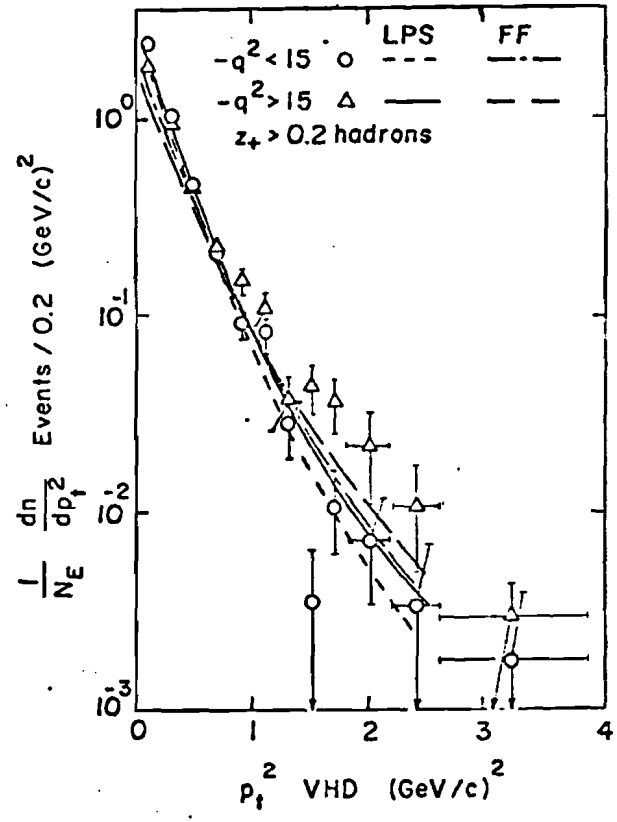

FIGURE 4-24

Distribution of transverse momentum squared from the VHD for forward jet hadrons, events separated into low and high W^2. LPS and FF model curves superimposed.

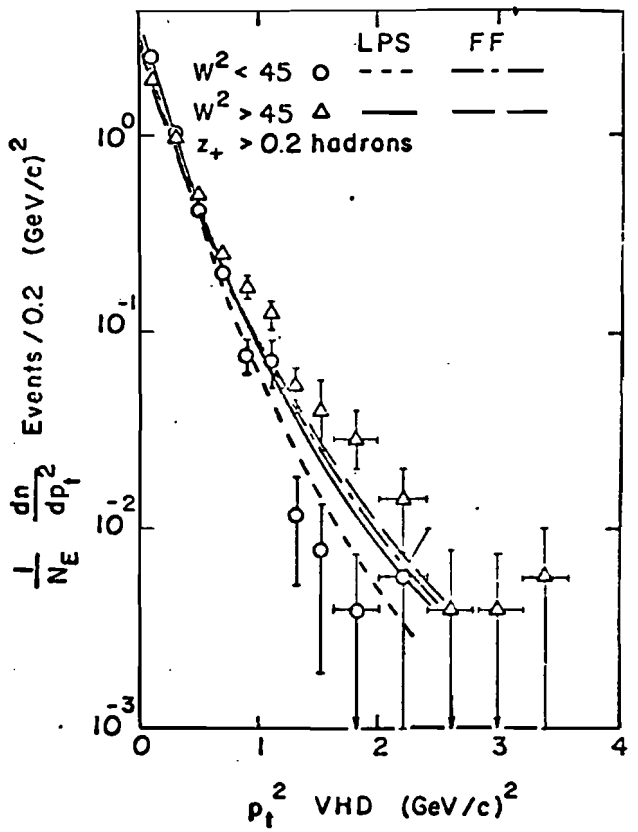

FIGURE 4-25

Distribution of transverse momentum squared from the VHD for backward jet hadrons, events separated into low and high $-q^2$. LPS and FF model curves superimposed.

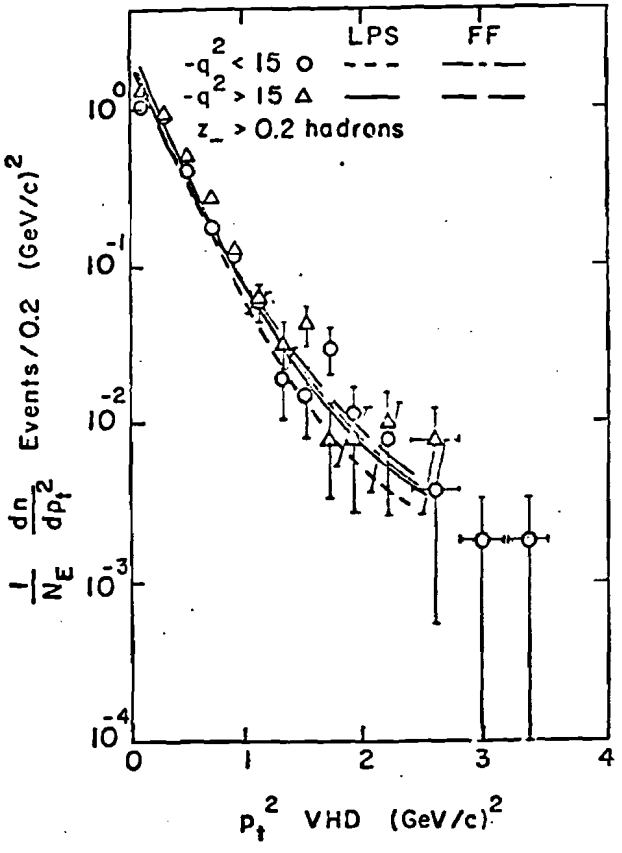

FIGURE 4-26

Distribution of transverse momentum squared from the VHD for backward jet hadrons, events separated into low and high W^2. LPS and FF model curves superimposed.

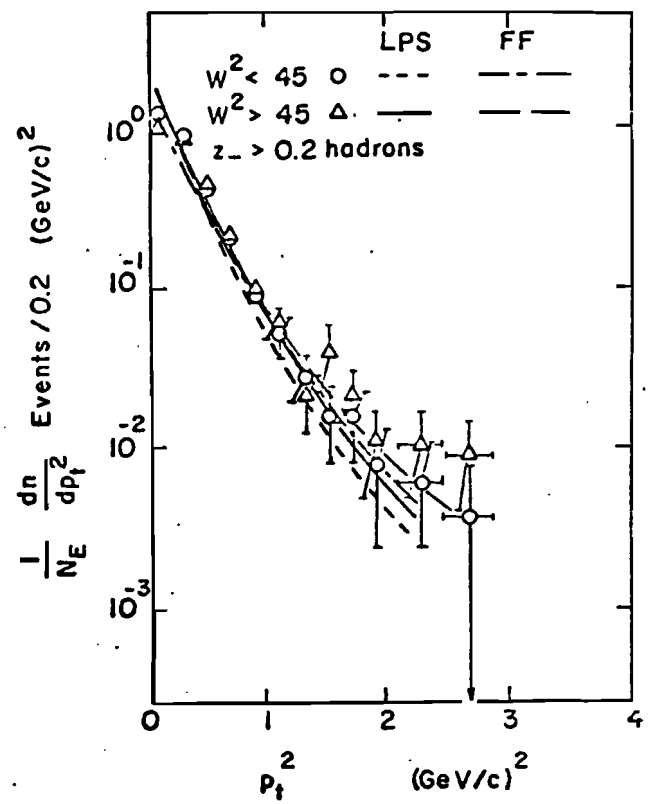

distributions, but this time for the backward jet hadrons. There is only a hint of higher p_t in the high $-q^2$ or high W^2 data, but as indicated by the LPS model, this is accounted for by the increased available phase space. Thus, the enhancement in the high transverse momentum tail at higher $-q^2$ or higher W is present primarily for the forward jet hadrons.

In Table 4-2 we present several fits to exponential forms for these various transverse momentum distributions. Although each distribution is reasonably consistent with the average (a "slope" to an exponential in the transverse mass of b = -5.8, for the distribution for all hadrons), there is a consistent trend favoring a broadening of the distributions at higher $-q^2$ and W^2, evident in the smaller (magnitude) "slope" parameters. The forward hadrons even indicate the reverse trend in q^2. These values can be compared with the similar ones given in references [IV-8, IV-11, III-7], and to the several distributions in reference [IV-13].

In order to emphasize the q^2 and W^2 dependence, we display the average values of p_t^2 for the forward and backward jet hadrons as functions of $-q^2$ and W^2, figures 4-27 and 4-28. These distributions provide the strongest indication of the effect we are examining; the average values of p_t^2 for the backward jet hadrons are well described by phase space considerations (as evidenced by the LPS model), but the forward jet hadrons clearly contain larger p_t on average

TABLE 4-2

Fits of Transverse Momentum Distributions to the Form $\exp(-b*m_t)$

Values of the Parameter "b"

	$-q^2 < 15$	$-q^2 < 15$	all $-q^2, W^2$
all hadrons	5.8 ±1.6	5.5 ±1.6	5.8 ±1.6
$z_+ > 0.2$ hadrons	4.7 ±1.7	4.1 ±1.7	4.5 ±1.7
$z_- > 0.2$ hadrons	4.2 ±1.8	4.8 ±2.0	4.6 ±1.9
	$W^2 < 45$	$W^2 < 45$	
all hadrons	6.3 ±1.7	5.3 ±1.6	
$z_+ > 0.2$ hadrons	5.4 ±1.9	3.9 ±1.7	
$z_- > 0.2$ hadrons	4.8 ±1.9	4.2 ±1.8	

FIGURE 4-27

Average p_t^2 versus $-q^2$ for forward jet and backward jet hadrons; 4-27a p_t^2 from LP, 4-27b p_t^2 from VHD. LPS and FF model curves superimposed. Data from ref [IV-11] is included.

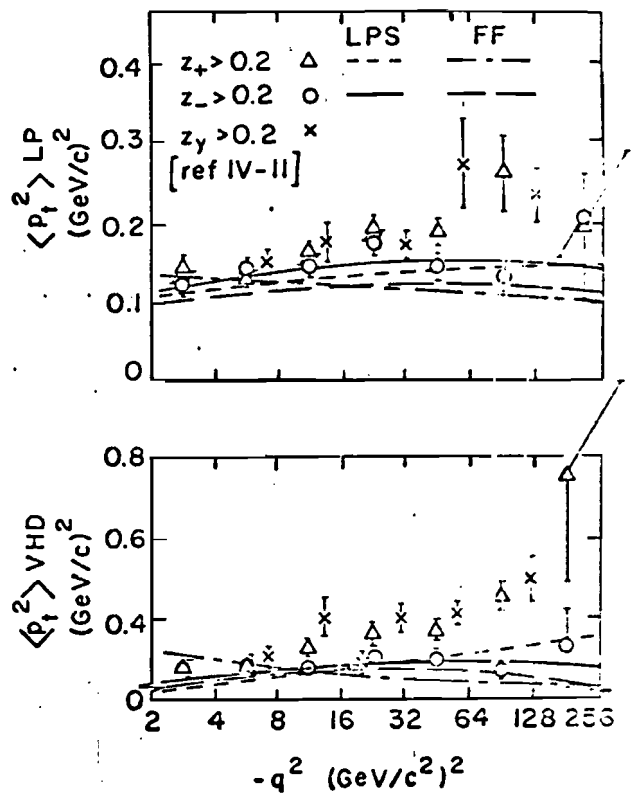

FIGURE 4-28

Average p_t^2 versus W^2 for forward jet and backward jet hadrons; 4-28a p_t^2 from LP, 4-28b p_t^2 from VHD. LPS and FF model curves superimposed. Data from ref [IV-11] is included.

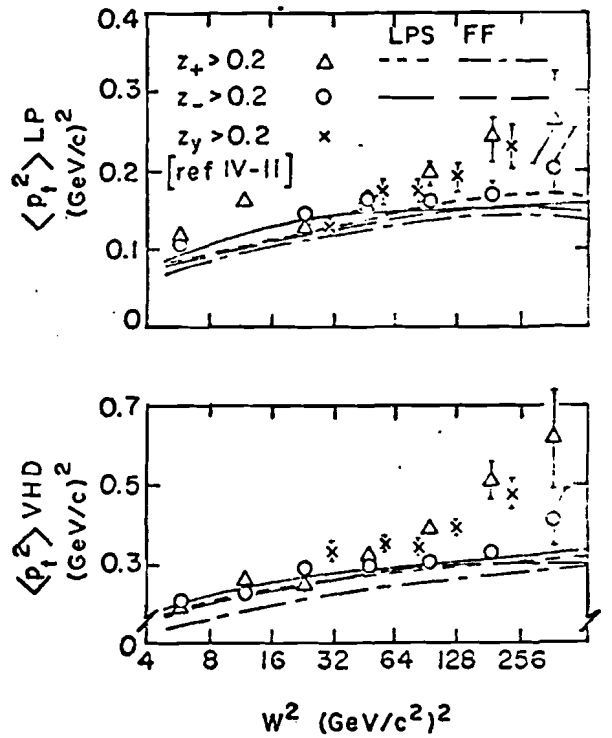

than is expected. Similar results are given in references [IV-11, IV-13, III-7].

We explore the forward and backward aspect of this asymmetry in p_t in figures 4-29 through 4-32. Here we plot average p_t^2 versus $-q^2$ and W^2, but with three different values of minimum z_+ and z_-. The backward hadrons do show a trend toward higher p_t^2 with increasingly higher minimum z_-, but this trend is well accounted for by the LPS model. The forward hadrons, however, show a significant rise in average p_t^2 as the forward requirement is strengthened, and always much in excess than the expectation based on the LPS model [IV-13].

Perhaps the most intuitive manner of displaying this forward-backward asymmetry in p_t is via a variant of the "seagull" plot [IV-15]. In figures 4-33 and 4-34 we display $\langle p_t^2 \rangle$ as a function of z_+ and z_-, in the two event samples separated by q^2 and W^2, but with the z_- data plotted inverted and adjoined to the z_+ data. The low $-q^2$ and low W^2 data are consistent with symmetry between the forward and backward hadrons (the usual, symmetric seagull), but for higher $-q^2$ and higher W^2 the forward hadrons have much higher average p_t^2 values than either the backward hadrons or the LPS model.

It has been suggested that the $\langle p_t^2 \rangle$ dependence on the fragmentation fraction z has a form

$$\langle p_t^2 \rangle = \langle p_t^2 \text{ frag} \rangle + z^2 * (\langle p_t^2 \text{ prim} \rangle + \langle p_t^2 \text{ QCD} \rangle) \qquad (4\text{-}4)$$

[IV-17, IV-18], where "frag" refers to the contribution to

FIGURE 4-29

Average p_t^2 from the VHD versus $-q^2$, for three values of minimum z_+. LPS model curves superimposed.

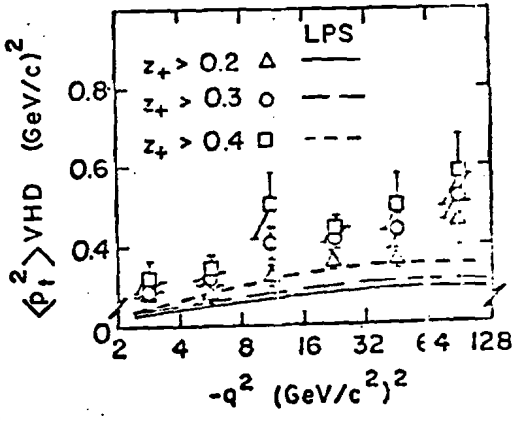

FIGURE 4-30

Average p_t^2 from the VHD versus W^2, for three values of minimum z_+. LPS model curves superimposed.

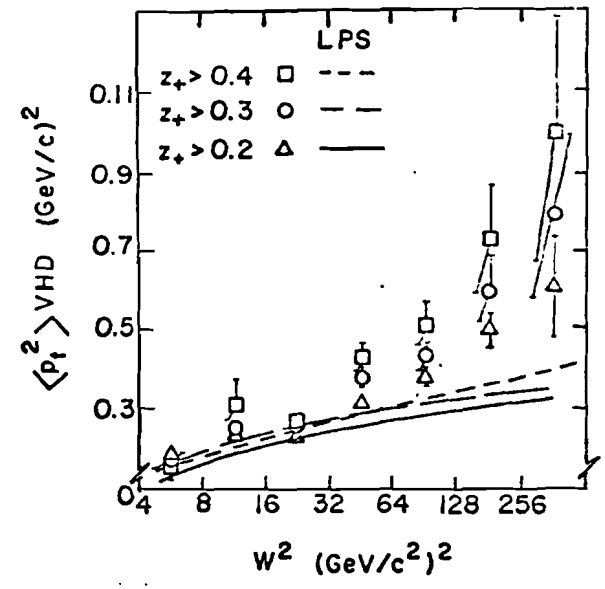

FIGURE 4-31

Average p_t^2 from the VHD versus $-q^2$, for three values of minimum z_-. LPS model curves superimposed.

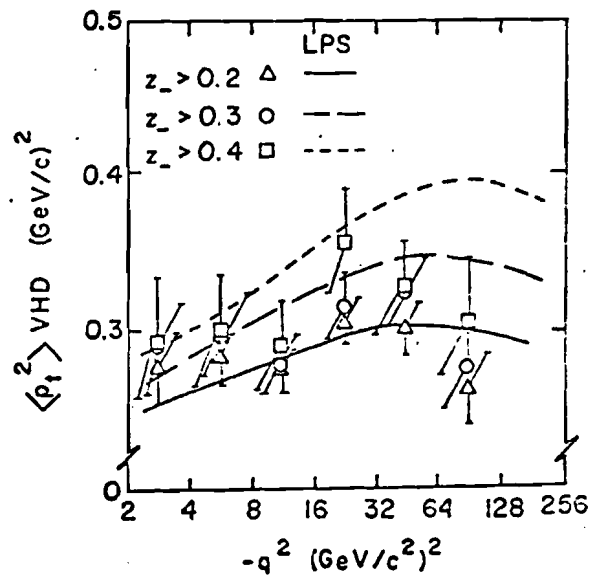

FIGURE 4-32

Average p_t^2 from the VHD versus W^2, for three values of minimum z_-. LPS model curves superimposed.

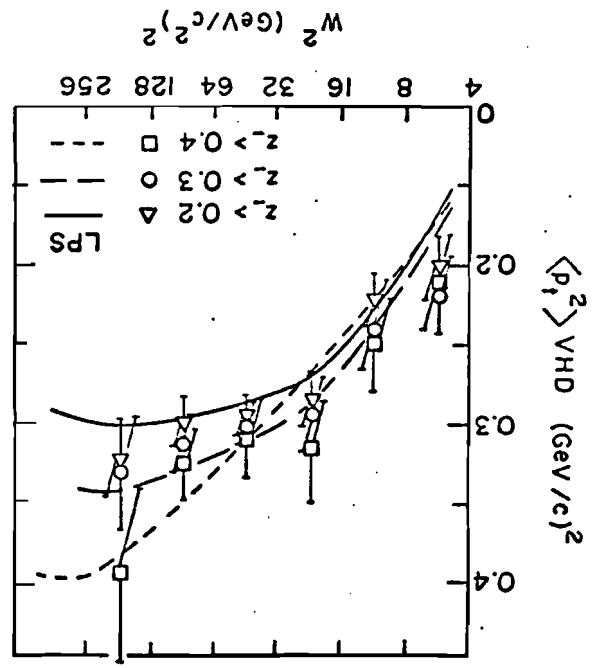

FIGURE 4-33

Seagull versus $-q^2$. Average p_t^2 (VHD) versus z_+ and z_-, plotted in "seagull" fashion, for low and high $-q^2$ events. LPS model curves superimposed.

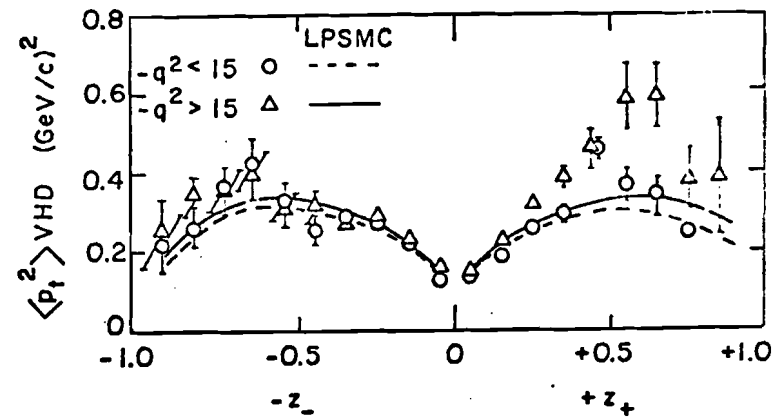

FIGURE 4-34

Seagull versus W^2. Average p_t^2 (VHD) versus z_+ and z_-, plotted in "seagull" fashion, for low and high W^2 events. LPS model curves superimposed.

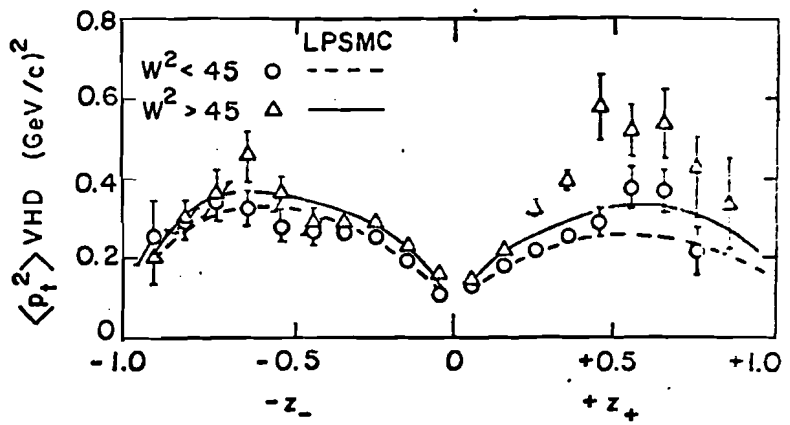

a hadron's transverse momentum from the process of quark fragmentation, "prim" refers to that contribution from the transverse momentum of the quark in the parent nucleon before the scatter with the lepton, and the "QCD" term comes from processes calculable by that theory. Both of the z^2 terms may have a dependence on q^2 or W^2 or both. We have tried such fits to our data, using both z_+ and z_-. (We note that the LPS-generated seguls, although forward-backward symmetric, still have z dependence to $\langle p_t^2 \rangle$, and, of course, this does not arise from either of the two sources mentioned in equation 4-4.) Unfortunately, the effects of phase space dominate the seagull plots to such a degree that such fitting is unsuccessful; that is, the chi-squared values obtained in most of these fits is quite large, indicating that the data really cannot be well approximated by such a quadratic form. In fact, reference [IV-18] suggests that such fitting be performed for data in which $W^2 > 100\ (\mathrm{GeV}/c^2)^2$, and such a restriction would leave us with very little data [IV-19].

As of yet, we have said little as to whether the source of high transverse momentum forward hadrons is dependent on q^2 only, W only, or both. We now investigate this, looking at the average values of p_t^2 as functions of q^2 and W^2 (figures 4-35 and 4-36), but now with the data restricted by the requirements $W^2 < 45$ and $-q^2 < 15$, respectively. The q^2 data is quite consistent with the LPS model; the W^2 data falls somewhat above the LPS curves, but not nearly as

FIGURE 4-35

Average p_t^2 versus $-q^2$ for forward jet hadrons only. All events with $W^2 < 45$ $(GeV/c^2)^2$. 4-35a p_t^2 from LP, 4-35b p_t^2 from VHD. LPS model curves superimposed.

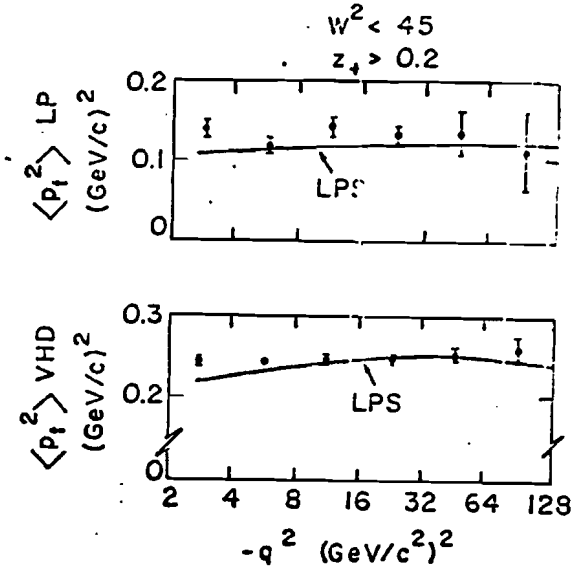

FIGURE 4-36

Average p_t^2 versus W^2 for forward jet hadrons only. All events with $-q^2 < 15\ (GeV/c^2)^2$. 4-36a p_t^2 from LP, 4-36b p_t^2 from VHD. LPS model curves superimposed.

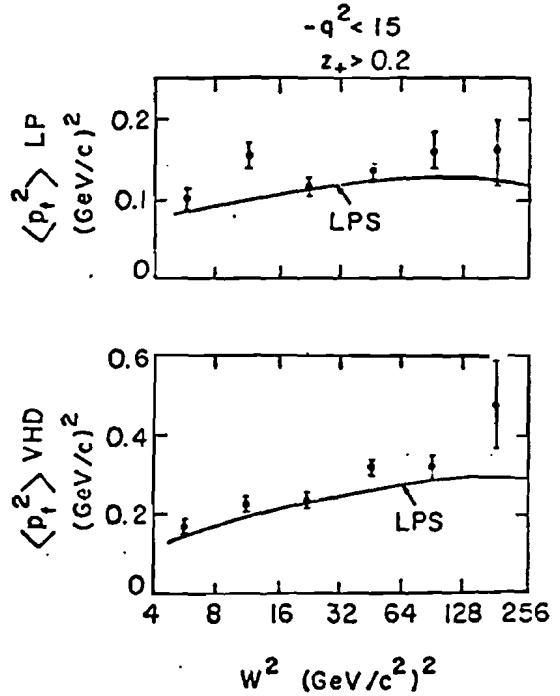

pronounced as in the earlier distributions, where there was no restriction on either variable. The data favor the hypothesis that the asymmetry is dependent mostly on W, and less on q^2, but the evidence in support of this is not strong. In figures 4-37 and 4-38 we show the complementary data, i.e. $-q^2$ dependence for high W^2 events and W^2 dependence of the high $-q^2$ events. Here the disagreement between the data and the LPS model is large for both, and somewhat larger for the W^2 dependence. Recalling the transverse momentum distributions, and the parameterizations of Table 4-2, we note a more pronounced change in the shape of the forward jet distributions when the data is divided according to the W^2 values than when $-q^2$ separates the data. The seagull shapes also favor W^2 as the variable where the high transverse momentum effect is best evidenced. So, although each of these comparisons individually are consistent with q^2 being as important as W^2, the combined effect favors W^2 as the more relevant variable.

Experimental Biases

We need to consider the effects of our measurement procedures and the peculiarities of the analysis we have performed as pertains to any possible enhancement or diminuition of the phenomena that we have just discussed.

The areas that we should be most concerned with are those aspects of the analsyis that will have particularly strong and/or equitable effects on the data. For example,

FIGURE 4-37

Average p_t^2 versus W^2 for forward jet hadrons only. All events with $W^2 > 45$ $(GeV/c^2)^2$. 4-37a p_t^2 from LP, 4-37b p_t^2 from VHD. LPS model curves superimposed.

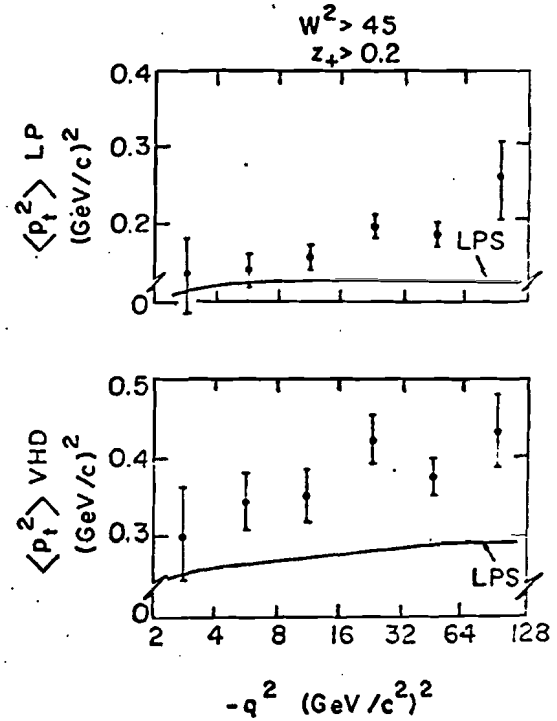

FIGURE 4-38

Average p_t^2 versus W^2 for forward jet hadrons only. All events with $-q^2 > 15\ (GeV/c^2)^2$. 438a p_t^2 from LP, 4-38b p_t^2 from VHD. LPS model curves superimposed.

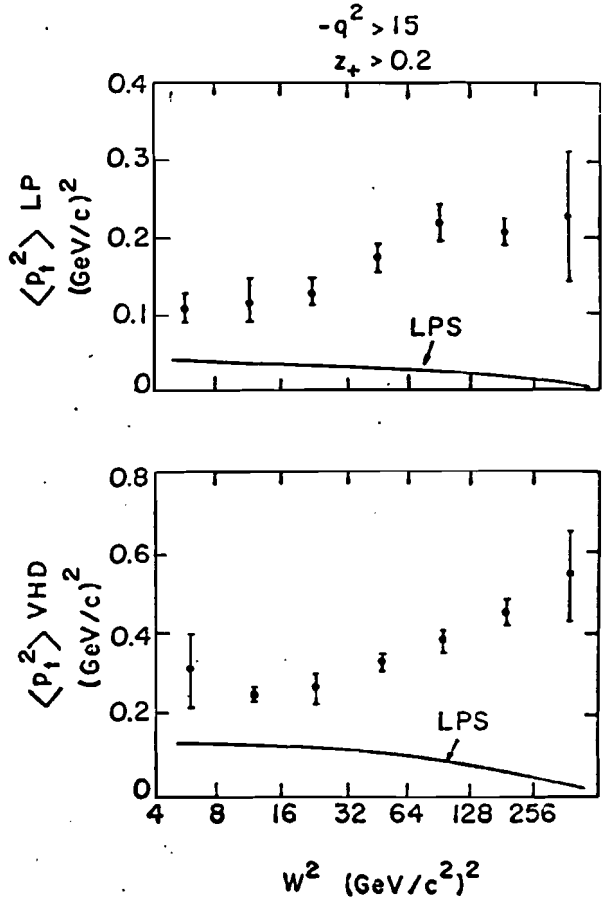

our concern is not so much with the uncertainty in determining the momentum of a hadron from a measurement of its curvature as with the possibility that this measurement is significantly more precise for low momentum hadrons than for the high momentum ones. Thus, we will pattern this discussion around the data that we have just displayed.

Before discussing several details of the analysis, we should again point out that a large fraction of the biases that our measurement precision or analysis procedures may introduce are also reproduced by both of the Monte Carlo simulations. In that these simulations, and particularly the LPS one, were the basis of comparison for all the experimental distributions, many of these biases have been accounted for because they affected data and simulation alike. Those aspects of the analysis and measurement that could not efficiently be reproduced tend to be rather unimportant.

The first topic we covered were the longitudinal momentum distributions, particularly the fragmentation functions. The analysis here is straightforward, with the momentum uncertainty the primary area of concern. The criterion that each hadron must be measured with a precision of 20 percent eliminates much of the uncertainty in these distributions; moreover, the simulations reproduced the momentum uncertainty of the measurement procedures. The z_- distributions are more susceptible to poor measurements than the z_+ ones, in that z_- involves differences of quantities that

are almost equal. However, for this and other reasons mentioned earlier, none of the subsequent analysis was particularly dependent upon the precise evaluation of z_-. As discussed previously, the major problem in these distributions (both that in z_- and that in z_+) is the existence of excess protons. Although an attempt was made to eliminate protons from those distributions whenever possible, the z_- distribution of positive hadrons indicates that this attempt was not entirely successful. Thus, the best way to insure that the results illustrated in the preceding sections are not seriously plagued by the excess protons is to examine only the negative hadrons. Several of the critical distributions that explored the high transverse momentum phenomena and the forward-backward asymmetry were reproduced using only negative hadrons, and the only observable difference was the obvious loss of statistics.

Transverse momentum distributions are also subject to hadron measurement uncertainties, but the same arguments used in the above paragraph apply here as well. A possible concern is the systematic bias that may be introduced by the incorrect choice of a longitudinal axis.

Transverse momentum measured relative to the lepton plane is free of this bias, and also tests the utility of the longitudinal direction that we employ. In figure 4-39 we display the momentum component of the total hadronic momentum vector perpendicular to the lepton plane. (Note that this is the actual component, positive or negative, and

FIGURE 4-39

Distribution of transverse momentum of the total hadronic system from the lepton plane. Mean = -0.00017 GeV/c, spread = 0.43 GeV/c.

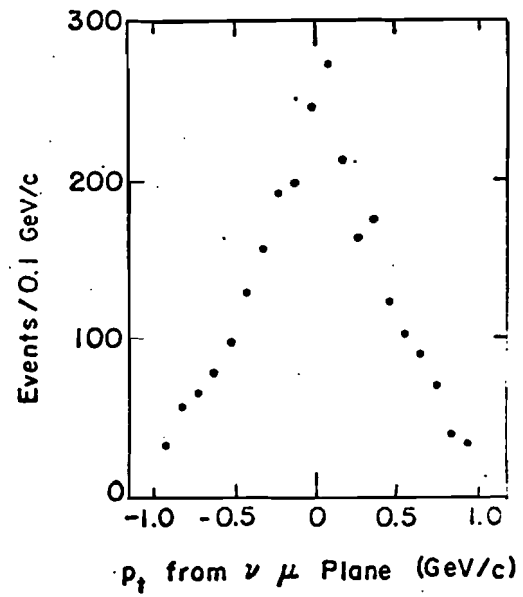

not the square or the magnitude.) The mean of -0.00017 GeV/c and width of 0.43 GeV/c indicate that there is no net bias in using the VHD as the longitudinal axis. Transverse momentum will also be affected by the measurement of the angle that the hadron emerges at. However, such measurements are typically quite good, and only become suspect for those very few hadrons which emerge at very large angles and often yield very poor stereo angles for reconstruction. These hadrons are few in number, and in any case, poor angular resolution will usually mean poor curvature resolution, which results in that hadron being deleted from the analysis.

Momentum is usually determined from curvature; however, the inverse relationship between momentum and curvature results in a statistical bias toward an overestimate of the hadron's momentum that is stronger for high momentum hadrons. Appendix B discusses an algorithm that we employ to eliminate such a bias. Consequently, when one examines the distribution of (fractional) momentum uncertainty as a function of momentum (where the momentum has been evaluated using this algorithm), there is an enhancement of larger fractional uncertainty at low momentum values. This enhancement is not big, but is unambiguous. We have experimented with reasonable variations in our hadron acceptance criteria, particularly with the form of this momentum determining algorithm, and with the value of the fractional momentum cutoff, and have observed no significant change in any of the

Moreover, the Monte Carlo simulations show similar characteristics, and so any indirect effects are reproduced there.

NOTES TO CHAPTER IV

IV-1 R. Heilman, CERN WA21-int-1 (1978)

IV-2 B. S. Yuldashev, et al., Acta Phys. Pol. B9, 513 (1978)

IV-3 T. H. Burnett, et al., Phys. Lett. 77B, 443 (1978)

IV-4 V. J. Stenger, Proceedings of the Topical Conference on Neutrino Physics at Accelerators, Oxford (1978) pg. 99

IV-5 J. Kogut, L. Susskind, Phys. Rep. 8, 75 (1973)

IV-6 F. W. Brasse, talk given at the XX International Conference on High Energy Physics, Madison (1980)

IV-7 J. Blietschau, et al., Proceedings of the International Conference on Neutrinos, Weak Interactions, and Cosmology, Bergen (1979) pg. 499

IV-8 J. Bell, et al., Phys. Rev. D19, 1 (1979)

IV-9 M. Derrick, et al., Phys. Rev. D17, 1 (1978)

IV-10 J. P. Berge, et al., Phys. Rev. D18, 3905 (1978)

IV-11 J. W. Chapman, et al., Phys. Rev. D14, 5 (1976)

IV-12 P. Bosetti, et al., Nucl. Phys. B149, 13 (1979) and H. Deden, et al., CERN preprint CERN/EP 80-66 (1980)

IV-13 C. Tao, et al., Phys. Rev. Lett. 26, 1726 (1980)

IV-14 J. J. Aubert, et al., CERN preprint CERN/EP 80-119 (1980)

IV-15 An alternative procedure for such a separation, relying on the variable $x_{||} = 2*p_{||} / W$, where $p_{||}$ is evaluated in the hadronic center of mass frame, has been investigated. The difference in this variable, compared with z_+ and z_-, is small (for $x_{||}$ away from zero), but requires a Lorentz boost which introduces unavoidable biases into the analysis.

IV-16 An excellent description of the "seagull" effect is given as one of the appendices in reference [IV-8].

IV-17 M. Gluck, E. Reya, Nucl. Phys. B145, 24 (1978)

IV-18 M. Gronau, Y. Zarmi, Phys. Rev. D18, 2341 (1978)

IV-19 We should point out that, because our longitudinal axis, the VHD, is not constrained to lie in the lepton plane, the contribution to $\langle p_t^2 \rangle$ from the "primordial" transverse momentum of the quark within the parent nucleon is greatly reduced. However, this does not affect the fitting procedure, and only indicates that the motivation (for reference [IV-18]) for performing such tests is perhaps not relevant to our data.

CHAPTER V

CONCLUSIONS

In this section we will discuss the results presented in Chapter IV and review them with respect to their interpretation.

Hadron fragmentation, as parameterized by the sums of fragmentation functions that we have presented, can be understood largely from the standpoint of kinematics and phase space considerations. This is evidenced by the fact that the LPS model gives reasonable reproduction of the fragmentation functions. (We are referring, of course, to the z_+ distributions; as discussed previously, the z_- distributions are not to be given much consideration.) The FF model describes the positive hadron distribution quite well, as might be expected when the hadron jet generation begins necessarily with a positively charged quark or antiquark. The negative hadron distribution is not so well modelled by the FF simulation, perhaps because the suppression of negative hadron formation in this model is strong. (We should note, however, that the disagreement is most apparent in the high z region, where even the models are uncertain.) Nevertheless, longitudinal momentum is distributed via a mechanism which does not change drastically within the range of the inclusive variables of this study, and does not differ much with the distribution obtained by employing momentum conservation,

limited transverse momentum, etc. alone.

The q^2 dependence of the positive fragmentation function is not expected based on either of the two models we have employed. Neither of these models has any such dependence, other than that very indirect connection based on differing available phase space [V-1]. The softening of the fragmentation function with increasing $-q^2$ is expected, however, from QCD processes [III-14, V-2, V-3]. Although hadron fragmentation is one of the least tractable topics for QCD, the qualitative effect is still expected. (Actual calculations performed predict only the change in fragmentation functions with q^2, or, equivalently, relationships between moments of fragmentation functions.) Naively, this is because at higher $-q^2$, when the probability of having a distinct gluon in the final state is larger, the subsequent (almost) independent fragmentation of the two partons will result in hadrons with less momentum each than if all the hadronic momentum were in a single fragmenting quark. This consistency of the data is far from a definitive statement in favor of QCD, however. We can only state that the data indicate a softening of the positive hadron fragmentation function with $-q^2$, which is in qualitative agreement with what one would expect if QCD-related processes were responsible for fragmentation.

The enhancement of high transverse momentum hadrons is also outside the realm of either of our models. Both models attribute p_t to hadrons based on distributions that depend

on $-q^2$ or W only in that the p_t given must not exceed the available energy. Again, QCD does predict that this high p_t phenomenon will arise with increasing $-q^2$ or W^2 [V-4, V-5, V-6, V-7, V-8]. This is because large angle emission of a gluon by the fragmenting quark is more likely to occur at large $-q^2$ or large W^2. Thus there is a large transverse momentum between the two partons, which gets transferred to the hadrons that are subsequently produced when these partons fragment. Fortunately, QCD can be more quantitative for this phenomenon. An analytic calculation for deep inelastic neutrino scattering with neutrinos of our average energy reproduces the high p_t tail of our transverse momentum distribution, and reproduces the $-q^2$ and W^2 dependence as well. Such curves, superimposed on our data, are illustrated in figures 5-1 and 5-2 [V-9].

Although this calculation has none of the details of our measurement or analysis procedures included, the agreement is still significant.

The final topic, that of the forward-backward asymmetry in the hadronic transverse momentum distributions, is closely related to the previous one. Neither model reproduces this phenomenon, and in fact, comparison with either model is meaningless in that neither model treats the forward and backward jets as distinct entities (unless, of course, the effect were due to analysis procedures, kinematics, etc.). Both models produce backward jet hadrons via the same

FIGURE 5-1

Distribution of transverse momentum squared from the VHD for all hadrons, separated into events with $-q^2 > 25\ (\mathrm{GeV}/c^2)^2$ and those with $-q^2 > 25\ (\mathrm{GeV}/c^2)^2$. Curves are that depicted by QCD [V-1].

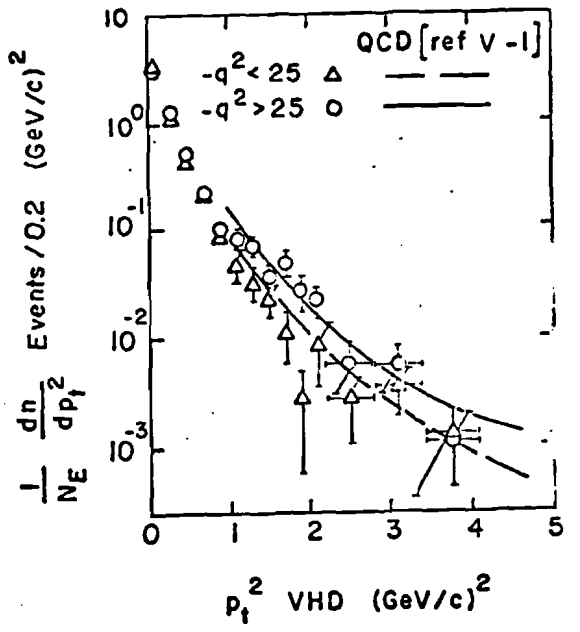

FIGURE 5-2

Distribution of transverse momentum squared from the VHD for all hadrons, separated into events with $W^2 < 50\ (GeV/c^2)^2$ and those with $W^2 > 50\ (GeV/c^2)^2$. Curves are that predicted by QCD [V-1].

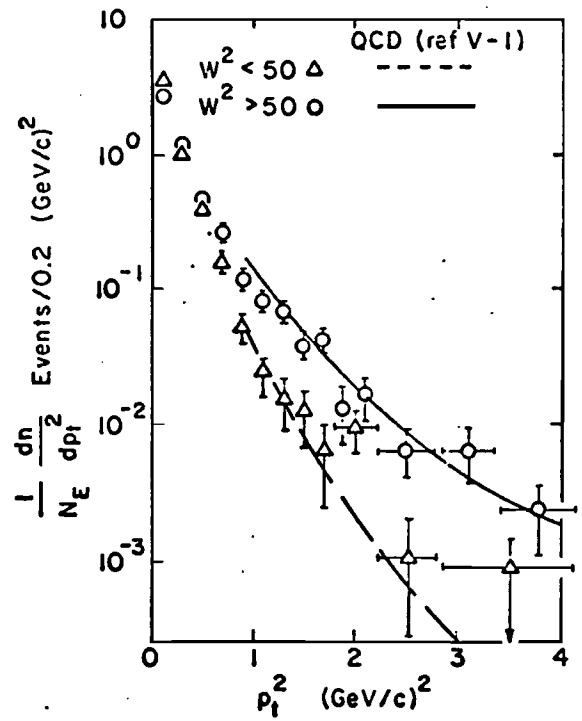

procedure that all hadrons are generated, and the classification of a hadron as to forward or backward is purely a matter of the amount of longitudinal momentum the hadron has. (The LPS model could be extended to treat the two jets distinctly; however, such an extension is really outside the spirit of this model. The FF model also could be extended to treat the fragmentation of the diquark system distinctly from the quark. However, in that this model is largely phenomenological, this would require the parameterization of diquark fragmentation.) The arguments based on QCD applied to the general topic of high p_t hadrons apply here as well; moreover, QCD does address the forward-backward comparison in related ways, which apply at least qualitatively to the results that we have shown [V-10, V-8]. However, the calculations performed are, again, incapable of properly treating the non-perturbative ('soft') contributions to transverse momentum, and so we can only note the qualitative agreement with our data.

In addition to the high transverse momentum forward-backward asymmetry that we have presented here, analysis of the shape of these high transverse momentum events has been performed, indicating a preference for the large transverse momentum to align itself in a planar, as opposed to cylindrically symmetric, orientation. This is highly suggestive of some process similar to the emission of a gluon that QCD describes. [V-10]

Independent of any theory, we can conclude the following: we have observed the longitudinal momentum distribution of the hadrons, as described by fragmentation functions, and have found them to be quite consistent with dependence primarily on phase space considerations, and with a mild softening that depends on $-q^2$; we have found that the transverse momentum distributions are also well described by phase space, except that there is a significant excess of hadrons at large values of p_t; the occurrence of these high p_t hadrons increases with increasing $-q^2$ or W^2; and, finally, when we categorize the hadrons as to association with either the forward jet or backward jet (viewed from the hadronic center of mass frame), it is the forward jet hadrons that display the $-q^2$ and W^2 rise in transverse momentum, while the backward jet hadrons behave according to the constraints of phase space. These results are all in qualitative agreement with the expectations of QCD, and where calculation is possible values exist, they are in reasonable quantitative agreement as well.

The uniqueness of this analysis lies in the novelty of the forward jet - backward jet comparison. Although previous experiments have analyzed the correlation between transverse momentum and longitudinal momentum, this has been in terms of the forward jet hadrons only. The ability of the bubble chamber to measure hadrons of all momentum well permits us to identify and analyze the backward jet hadrons.

This allows a comparison with the results from analysis of the forward jet hadrons, and enabled our discovery of the high $-q^2$ (high W^2) asymmetry of the transverse momentum distributions of these two jets.

NOTES TO CHAPTER V

V-1 The $-q^2$ dependence of D^+ and D^- is, as discussed in Chapter IV, due primarily to the neutrino scattering with the antiquarks more frequently at low $-q^2$ than for high $-q^2$. Thus, the actual fragmentation functions are not q^2 dependent, but the sums of the fragmentation functions that constitute D^+ and D^- are.

V-2 J. F. Owens, Phys. Lett. 85B, 67 (1978)

V-3 T. Uematsu, Phys. Lett. 79B, 97 (1978)

V-4 H. D. Politzer, Harvard Preprint HUTP-77/a038 (1977)

V-5 A. Mendez, Nucl. Phys. B145, 199 (1978)

V-6 A. Mendez, A. Raychaudhuri, V. J. Stenger, Nucl. Phys. B148, 499 (1978)

V-7 P. Mazzanti, R. Odorico, V. Roberto, Phys. Lett. 81B, 219 (1979)

V-8 M. D. Peccei, R. Ruckl, Max Planck Institute preprint MPI-PAE/PTh 26/80 (1980)

V-9 F. Halzen, Talk given at the XIth International Conference on Multi-particle Dynamics, Bruges, Belgium (June, 1980)

V-10 V. J. Stenger, talk given at the XX International Conference on High Energy Physics, Madison (1980)

List of References

G. Altarelli, G. Parisi, Nucl. Phys. B126, 298 (1977)

J. J. Aubert, et al., CERN Preprint CERN/EP 80-119 (1980)

H. C. Ballagh, et al., Phys. Rev. D21, 569 (1980)

J. Bell, et al., Phys. Rev. D19, 1 (1979)

J. P. Berge, et al., Phys. Rev. D18, 3905 (1978)

J. D. Bjorken, SLAC-PUB-1957 (1976)

J. Blietschau, et al., Proceedings of the International Conference on Neutrinos, Weak Interactions, and Cosmology, Bergen (1979) pg. 499.

P. Bosetti, et al., Nucl. Phys. B149, 13 (1979)

F. W. Brasse, et al., Proceedings of the XX international Conference on High Energy Physics, Madison (1980); to be published.

T. H. Burnett, et al., Phys. Lett. 77B, 443 (1978)

N. Cabibbo, Phys. Rev. Lett. 10, 531 (1963)

R. J. Cence, et al., Nucl. Inst. and Meth. 138, 245 (1976)

J. W. Chapman, et al., Phys. Rev. D14, 5 (1976)

H. Deden, et al., CERN preprint CERN/EP 80-66 (1980)

M. Derrick, et al., Phys. Rev. D17, 1 (1978)

A. DeRujula, et al., Rev. Mod. Phys. 46, 391 (1974)

J. Ellis, SLAC report #215 (1978)

J. Ellis, Proceedings of the 1979 International Symposium on Lepton and Photon Interactions at High Energies, Batavia (1979) pg. 412

R. P. Feynmann, Photon-Hadron Interactions, Benjamin Press (1972)

R. P. Feynmann, et al., Nucl. Phys. B128, 1 (1979)

R. D. Field, R. P. Feynmann, Phys. Rev. D15, 2590 (1977)

R. D. Field, R. P. Feynmann, Nucl. Phys. B136, 1 (1978)

M. Gell-Mann, Phys. Rev. 125, 1067 (1962)

M. Gell-Mann, Phys. Lett. 8, 214 (1964)

M. Gluck, E. Reya, Nucl. Phys. B145, 24 (1978)

M. Gronau, Y. Zarmi, Phys. Rev. D18, 2341 (1978)

F. Halzen, Proceedings of the XIth International Converence on Multi-Particle Dynamics, Bruges (1980); to be published.

R. Heilman, CERN WA 21-int-1 (1978)

J. Kogut, L. Susskind, Phys. Rep. 8, 75 (1973)

W. Marciano, H. Pagels, Phys. Rep. 36, 137 (1978)

P. Mazzanti, et al., Phys. Lett. 81B, 219 (1979)

A. Mendez, Nucl. Phys. B145, 199 (1978)

A. Mendez, et al., Nucl. Phys. B148, 499 (1978)

Y. Ne'eman, Nucl. Phys. 26, 222 (1961)

J. Orthel, Ph.D. Thesis, University of California, Berkeley; LBL-10035

J. F. Owens, Phys. Lett. 85B, 67 (1978)

M. D. Peccei, et al., Max Planck Institute preprint MPI-PAE/PTh 26/80 (1980)

S. Parker, et al., IEEE Transactions on Nuclear Science 25, 1 (1978)

D. H. Perkins, Rep. Prog. Phys. 40, 409 (1977)

D. H. Perkins, SLAC report #215

H. D. Politzer, Harvard preprint HUTP-77/A038 (1977)

A. Salam in Elementary Particle Theory, ed. by N. Svartholm, Almquist and Wicksell (1969) pg. 367

N. Schmitz, Proceedings of the 1979 Internation Symposium on Lepton and Photon Interactions at High Energies, Batavia (1979) pg. 359

V. J. Stenger, Proceedings of the XX International Conference on High Energy Physics, Madison (1980); to be published.

M. L. Stevenson, Proceedings of the Topical Conference on Neutrino Physics at Accelerators, Oxford (1978) pg. 99

C. Tao, et al., Phys. Rev. Lett. 26, 1726 (1980)

T. Uematsu, Phys. Lett. 79B, 97 (1978)

B. S. Yuldashev, et al., Acta Phys. Pol. B9, 513 (1978)

APPENDIX A:

The Two-Plane External Muon Identifier

Experiment 546 was the first bubble chamber experiment to employ the expanded 2-plane EMI [II-2, II-3]. An improvement over the original, the 2-plane EMI consists of 18 delay line readout multiwire proportional chambers in the first plane, 21 in the second, and the associated electronics to amplify, digitize, and record the MWPC data. In addition, 18 smaller wire chambers were installed in a fledgling Internal Picket Fence [A-1], but this data was not employed for the experiment.

The layout of the EMI and the bubble chamber is displayed in figure 2-2, and a schematic of the EMI system is displayed in figure A-1. The passage of a charged particle through the sensitive region of a MWPC can induce pulses on each of the three delay lines (one vertical, one horizontal, and one at a 45 degree angle). The position of these pulses, which yields the position of the particle passage, can be determined by recording the time taken for the pulses to reach the amplifiers at the ends of the delay lines. Such pulses were amplified and digitized as to time of arrival, and recorded on magnetic tape. On-line monitoring and data acquisition was facilitated through the use of a PDP-11 computer.

The data so recorded corresponds to the times of arrival of the various pulses from the delay lines of the MWPC's.

An off-line program, EMIKE, reconstructed the actual times and positions, using known pulse velocities of the delay lines. As many as seven pulses could be recorded for a given hit in a chamber, to be used for a determination of the time and position (in the two dimensions of the MWPC). Thus, reconstruction involved a four constraint fit. Inefficiencies, random hits, concidences, etc. required us to utilize 3C, 2C, and 1C fits as well in muon identification [A-2].

The major limitation in the EMI for identifying muons is due to the requirement that the muon candidate pass through so much absorptive material (7-10 absorption lengths). This limits the minimum momentum muon that can be identified to one with approximately 4 GeV/c in the direction of the EMI. For muons with momentum higher than this, the primary limitation is the geometric coverage of the two planes of MWPC's. This results in an 85 percent acceptance for negative muons. Other sources of losses are negligible, and of little concern for this analysis. Sources of false muon identification can be largely eliminated by a few simple kinematical constraints placed on the muon candidate. These are discussed in Appendix B. A thorough discussion of the EMI, as pertains to the validity of its muon identification, can be found in references [II-4, II-5].

NOTES TO APPENDIX A

A-1 M. L. Stevenson, Proceedings of the Topical Conference on Neutrino Physics at Accelerators, Oxford (1978)

A-2 In fact, the upgrading of the EMI was not completed for this experiment; thus, some MWPC's could only produce a maximum of 6 encodings per hit, or a 3C fit.

APPENDIX B:

Selection of Event Sample and Analysis Procedures

Charged Current Event Identification

All potential muon tracks found in the scan for neutral induced interactions were measured. These measurements were reconstructed and extrapolated to the two planes of wire chambers that constitute the EMI. Comparison between the extrapolated position and the positions of real hits in the EMI determined the charged current events. The precise criteria that must be met for classification of a charged current event are as follows:

Primary vertex location: the primary vertex must be located within a restricted volume within the bubble chamber. This volume can be generally described as that region within 110 cm. of the chamber equator, greater than 5 cm. from any wall, and further than 70 cm. from the downstream wall (to insure room for the measurement of the hadron system within the bubble chamber). The event must be visible from all three camera angles.

Muon track: the muon candidate must have a trajectory within the bubble chamber characteristic of a muon, i.e., no large scatters or interactions (the loss due to inelastic muon-nucleon scattering is negligible), no electromagnetic showers, etc. This track must have greater than 4 GeV/c momentum in the neutrino direction. The measured length must exceed 70 cm.

EMI Match: The two solutions that are matched to the extrapolation positions from the reconstructed track must have resulted from at least 4 encodings each (as many as 7 are possible). They must have times within 350 nsec of one another. The closeness of the fits between hit and extrapolated positions are measured by a 4 degree of freedom chi-squared and a corresponding probability. That is,

$$p = (1 + \chi^2) \exp(-1/2\ \chi^2)$$

$$\chi^2 = \chi_x^2 + \chi_y^2 \qquad \text{(B-1)}$$

$$\chi_x^2 = (\Delta X_1, \Delta X_2)\ C(X_1, X_2)\ (\Delta X_1, \Delta X_2)$$

χ_y^2 is similar to χ_x^2; the covariance matrix is determined almost wholly from the uncertainty in the extrapolation and this is primarily due to Coulomb scattering and the momentum uncertainty of the reconstructed track. $(\Delta X_1, \Delta X_2)$ corresponds to the difference in the EMI hit position and the extrapolated position for the (1st, 2nd) plane. The probability, p, that results must exceed 1 percent.

Selection of Analysis Sample

Only a subset of all the identified charged current events were fully measured for this analysis. Those events fully measured were not always employed, as the interpretation of some events can either be difficult, or incompatible with the processes that are to be investigated. The actual event sample used were selected according to the following criteria.

The projection of the muon's momentum in the plane perpendicular to the neutrino direction was required to be greater than 90 degrees from that same projection of the total hadronic momentum. This requirement was imposed to eliminate a small background of misidentified charged current events, where a hadron masquerades as a muon.

The correction factor, "g", by which the hadronic energy is scaled to compensate for that component of the hadronic energy lost in undetected neutral hadrons, must be less than 3. This requirement eliminates those events for which our estimate of the neutrino energy, and therefore $-q^2$, W etc. is too uncertain.

The kinematic region of interest requires that we avoid events where the hadronic system is likely to be dominated by the effects of resonance production or other nonscaling phenomena. Moreover, we would like to insure that there is enough available energy in the hadronic system to permit its development without being dominated by momentum and energy conservation. Thus, we require

total hadronic energy > 10 GeV

$-q^2 > 2\ (\mathrm{GeV}/c^2)^2$

$W > 2\ \mathrm{GeV}/c^2$

Event Measurement

Events were measured using a set of guidelines [B-1] that were formulated on the basis of previous neutrino-nucleus

experiments [B-2]. The emphasis of these rules was to determine the incident neutrino energy and analyze the characteristics of the produced hadrons. The charged hadrons can be easily analyzed; analysis of the neutral hadrons is much more difficult, and so the spirit of the measurement and analysis was to regard the neutral hadron induced secondaries as important primarily for the determination of the total hadronic energy. Thus, these measurement guidelines stated, in brief, as follows.

All charged tracks from the primary vertex are to be measured.

All vees, or neutral strange particle decays ($K^0_s \rightarrow \pi^+ \pi^-$ or $\Lambda \rightarrow p\pi^-$), and all neutral hadron interactions that are consistent with the neutral hadron originating from the primary vertex are to be measured.

All photon materializations (gamma $\rightarrow e^+ e^-$) within two radiation lengths of and consistent with pointing to the primary vertex are to be measured.

All particles originating from a secondary scatter, interaction, etc. that is the endpoint of a measured track must also be measured if this secondary vertex occurs so soon on the length of the track (relative to that track's curvature) that the uncertainty in the curvature of the track is greater than 25 percent.

In the above, the estimate of whether a neutral induced secondary vertex is consistent with a primary vertex origin for the neutral hadron was a subjective one. Neutral hadron interactions, which cannot be proven to originate at any place, were measured when they fell within a 45 degree cone of the neutrino direction centered on the primary vertex. Vees and gamma materializations were measured liberally, since either kinematic fitting or pointing algorithms would later determine which actually are related to the primary vertex.

Analysis Specifications

Detector limitations and measurement imprecision often require that one estimate quantities of interest. Several choices have been made for such estimations, discussed below. Possible biases that would result from these choices are discussed, as appropriate, in chapter 4. These choices are as follows.

Determination of particle momentum. The magnetic field that surrounds the bubble chamber bends the trajectories of charged particles according to the momentum of the particle and the angle it makes with respect to that field. However, the algorithm for reconstructing the track's trajectory and determining the momentum treats curvature (in units of 1/momentum) as the relevant variable, along with the two angles. In that the mean value of the inverse of a quantity is not a large sample of measurements will not be correctly

determined from the curvatures. To minimize this bias, we have instituted a variation of the usual momentum determination procedure, based on including the next term of an expansion of momentum as a function of curvature and its uncertainty. Specifically, for any charged track whose momentum is to be determined from curvature, that momentum value is given by

$$p = 1/\sqrt{k^2 + (\Delta k)^2} \qquad \text{(B-2)}$$

where k, Δk are the curvature and uncertainty in curvature, respectively. For those tracks whose fractional momentum uncertainty is greater than 25 percent, and thus have the tracks from its downstream vertex measured, the momentum (magnitude) is determined by adding the momenta of the secondary tracks and scaling this up by 20 percent to account for the expected loss of neutral hadron energy. The direction, of course, can be determined quite well from a straight line between the upstream and downstream vertices. (We note that, in that the emphasis of the analysis centers on high transverse momentum hadrons, this procedure will yield an accurate determination of the angle at which the hadron is produced, and a lower limit to the hadron's momentum, and therefore only detract from, and never enhance, the effects we are concentrating on.)

Particle identification. In general, particle identification is not possible for this experiment. Muons can be determined in most cases (see Appendix A and ref [II-4, II-5]),

and only events for which precisely one muon exists are examined. Whereas electron identification is often imprecise, we expect few primary electrons, and misidentification of tracks from neutral induced secondaries is not important. Separating protons from positive pions and kaons is usually possible only for low momentum tracks, when the hadron slows enough to identify itself, either by the heavier bubble formation (due to heavier ionization) or if the hadron stops within view of the cameras. Using an approximate range-energy relationship,

$$R = 200 * p^{3.32} \text{ (R in cm., p in GeV/c)} \qquad \text{(B-3)}$$

which is an approximation to the range-energy relationship we have analytically calculated B-3 , we see that a 500 MeV/c proton travels 20 centimeters before stopping, and a 1 GeV/c proton travels 2 meters. Thus, for any proton with momentum higher than a few hundred MeV/c, visual identification is unlikely. Previous studies [IV-2, IV-3] have also found that above this momentum range proton identification is very uncertain. Thus, although we do attempt to identify protons, we are not really capable of such identification for all but the low momentum protons. Similarly, identifying other hadron species, i.e. separating pions from kaons, is rarely possible. For all exclusive distributions that we study here, we will only distinguish the hadrons according to electric charge. (Neutral strange particles can, in general, be identified in the bubble

chamber; however, in that we are only concerned with the charged hadrons, such identification is of no value.)

Inclusive quantities are determined in a straightforward fashion, with virtually the sole source of error due to the uncertainty in determining the neutrino energy. Given this quantity (the estimation procedure for the neutrino energy is described in Chapter 4), one defines:

$$\begin{aligned} q^2 &= (k - k')^2 \\ W^2 &= (q + P)^2 \\ x &= -q^2/2*(P\cdot q) \\ y &= q\cdot P/k\cdot P \end{aligned} \qquad \text{(B-4)}$$

where the four vectors k, k', and P refer to the neutrino, muon, and target, respectively.

The definition of rapidity, transverse momentum, fragmentation variables $z_\pm$, etc. all rely on an estimation of the direction of the quark after it is struck, which is presumably that of the total hadronic system. Here the loss of neutral hadrons again plagues the analysis. It has been determined [IV-8] that a relatively unbiased estimator of this direction is given by the sum of the momenta of all charged primary hadrons with all related neutral-induced secondary vertices. For the purpose of examining the transverse momentum distributions, this will yield an underestimate, as this axis minimizes transverse momentum of the tracks in an event. The effect on longitudinal distributions will be small, as the transverse momentum is usually only a

small fraction of the total momentum and thus not a large source of error.

For the exclusive distributions, all primary hadrons that are not positively identified as protons are candidates for the analysis. Measurement errors, particularly the uncertainty in the momentum, are usually ignored, unless they are large. Specifically, when the momentum is uncertain enough (fractional uncertainty in curvature > 20 percent), or the geometric reconstruction for the track yielded an uncertain fit (RMS deviation > 30 microns on film), the track was deleted from the distributions considered. Note that this is not the same as deleting the track from the analysis, as it is still used in determining the inclusive quantities and the total hadronic direction (presumably the large fractional momentum uncertainty of a single track will not induce a large fractional momentum uncertainty in the total hadronic momentum). We have experimented with these cuts, observing the effects of changing the values individually, and have found that our results are relatively insensitive to reasonable variations.

The definition of the fragmentation variable is somewhat arbitrary, in that several definitions have been used, yielding similar results. We have employed z_+ and z_-, given by equation (4-3), viz.

$$z_\pm = (e+p_{||})/(E+P_{||})$$

where $(e,p_{||})$ and $(E,P_{||})$ refer to the hadron, total hadronic system energy and longitudinal momentum, respectively.

We have also used a definition based on the ratio of longitudinal components of the individual hadron's momentum with the total hadronic system momentum, and found virtually indistinguishable distributions with respect to z_+.

NOTES TO APPENDIX B

B-1 University of Washington Internal report VTL-ON-78 (1978)

B-2 Each of the research groups participating in this experiment have previously been involved in one or more similar experiments using neutrino and/or antineutrino beams in the FNAL 15-foot bubble chamber.

B-3 G. Swider, University of Washington Internal Report VTL-HEP-44.

APPENDIX C

Monte Carlo Simulation

Neutrino-nucleon interactions have been simulated via Monte Carlo techniques according to two different models. One model, which has been termed 'longitudinal phase space', mimics only very general properties of hadronic jets in simulating these interactions. The other, based on the model of hadronic jets by Field and Feynmann (discussed in Chapter 3), uses that specific iterative hadron generating scheme, adapted for this experiment, to produce its own 'events' for analysis.

The general structure of both of these simulations is oriented toward comparing distributions from these models to those from our data. For this comparison to be valid, one must insure that any discrepancies between two versions of some distribution are due only to the differences between the way that the model describes the relevant process and the way that process actually happens in the experiment. This means that any effects that our measuring and analysis procedures have must either be eliminated or similarly introduced in the simulation. We have chosen the latter path by producing measured events via our simulations, and processing these 'events' through the exact same analysis as the data. The primary sources of discrepancies avoided by this procedure are those that would result from the bias introduced by the

acceptance of the EMI and those that would result from the neutrino energy estimation procedure. (The selection of events with muon transverse momentum greater than 4 GeV/c is also mimicked, so that this effect is present in the simulation results as well.)

This procedure in itself is not enough. Inventing data at the post-measurement stage does not exclude all biases due to the event selection and measurement procedures. Of particular importance here are the effects of measurement errors and of not observing all of the particles in an event. To mimic these effects, our simulations include the following. The events simulated are actually positioned in the bubble chamber, with the selection of the primary vertex according to a uniform distribution. The same routine that determines whether an event is within our prescribed 'fiducial volume' for the real events is also applied to the simulated ones. Once positioned in the chamber, the same algorithms used to reconstruct a real event within the bubble chamber from the three projections that the cameras record are now employed in reverse to insure that the simulated event could have come from images on film that our scanning and measuring procedures would process. If this primary vertex position is established as a valid one, we use it for further cross-checks. Primary vertex tracks are assigned a length which is the smaller value between the distance to the chamber wall and

the expected distance to an interaction (selected so as to yield the interaction probability for the neon-hydrogen mixture and the particle momentum). As this estimates the length that a real track would be measured, the momentum uncertainty can be determined. The values of the momentum and angles that are actually used are based on the model-determined momentum and the track length, randomly varied to simulate the expected gaussian distributions in curvature and angles. The simulation of photons produced by neutral pions uses the primary vertex position to determine whether the photon conversion occurs within the bubble chamber. Electron pairs are created and included in the measurement record when this happens, as are pion pairs from K^0 decays and pion-proton pairs from lambda decays.

In this way, several of the inefficiencies and/or sources of error inherent in our event selection, measurement, and processing system are imposed on the simulated events. Several other sources, however, are not. Hadronic interactions are difficult to model, and are neglected. Thus primary hadrons in the simulated events will never be ascribed a momentum value based on summing the momentum of the secondary hadrons from the primary hadron's downstream interaction, (which can happen for hadrons from the real events). Similarly, neutral hadron interactions are never included in the energy estimation algorithm for the simulated events. Brensstrahlung for electrons is ignored, so the

momentum determination for simulated events' electrons is more precise than that of real events' electrons. Moreover, no unrelated pairs from photons (from bremsstrahlung or other sources) can be included in the energy estimation algorithm in simulated events. These differences are rather small if suitable precautions are taken in the analysis procedures; their effects, and the precautions taken are discussed where appropriate in Chapter 4.

We will briefly discuss each of the two simulations below. A more complete explanation of both is given in reference [III-9]. In both, the neutrino spectrum used for generation of the events is that calculated for the configuration used in our data collection run [II-1].

Longitudinal Phase Space

The LPS model is basically a scaling model. The values of x (the momentum fraction of the struck quark) are selected according to a parameterization of measured structure functions. The inelasticity values, y, are chosen to be uniform, and the values of q^2 and W are calculated from the neutrino energy and x and y.

The hadronic system is created using three assumptions: the multiplicity of hadrons is chosen to follow a linear dependence on the logarithm of W (with one third of the hadrons neutral an average); the longitudinal momenta are selected such that the rapidity values are uniformly distributed within the kinematically allowed range; and the

transverse momenta are chosen to yield an exponential behavior, depending on the transverse mass and having a 'slope' parameter of b= -6. Of course, conservation of charge, momentum, and energy are enforced, which often significantly alters the momentum selections made according to the above specifications.

One can see that this model will be useful in distinguishing which characteristics of the data are due to the limits imposed by kinematics and finite neutrino energy, coupled with a hadronic system that evolves with only very general jet-like properties. As the term phase space implies differences between this simulation and real data can be ascribed to the underlying dynamics of the process being studied.

The major inefficiencies of this simulation are primarily those involved with measurement difficulties. In that real data come from measurements of film, measurement uncertainties related to stereo angles, film imperfection, and reconstruction affect the data in a fashion that is not easily reproduced. Problems associated with nuclear effects (the bubble chamber fill is neon and hydrogen) are not reproduced, either. However, these problems are relatively small, and can be minimized by more stringent measurement requirements.

Field and Feynman Model

The nature of this model is discussed in Chapter 3, and of course, in ref [III-9, III-10, III-11]. Here we will only discuss the particular fashion in which the model

was employed.

Implementation of this model is straightforward as concerns the jet related to the struck quark. Any hadronic processes related to the remnants of the target nucleon are beyond the scope of the model, and so actual use requires that the user develop a method for dealing with the target. We have employed a simple-minded procedure here, which involves reforming a baryon using the target remnant and the very last quark which can no longer fragment according to the model because of insufficient energy. This baryon contains the remaining momentum and energy, and is selected to be the simplest baryon that contains that assemblage of quarks. Thus, only protons, neutrons, lambdas, positive sigmas, and the doubly charged 'delta' resonance (1282) are formed. (No other resonance need be considered because at least one 'up' quark will always remain.) Of course, the delta is decayed, and the lambda treated in the appropriate fashion for a neutral strange particle. In the case of an antiquark scattering with the neutrino, 4 quarks will remain, and the final jet-related parton will be an antiquark. A meson and a baryon are then produced, with quark content and momentum content of each arbitrarily shared.

Vector mesons are produced in this jet generation scheme, as are pseudoscalar mesons that have a short lifetime. The decays of such mesons are handled in a straightforward manner, including all final states that have a

branching ratio of 10 percent or more. Sequential decays are properly created; e.g. production of a K* requires that its decay be modeled, which can result in a K^0_s which must then be decayed, sometimes yielding two neutral pions that then are decayed, etc.

The efficiencies of this simulation are basically the same as those of the LPS simulation. The rather unmotivated fashion employed for terminating the hadron generation iteration will mean that one should not seriously consider any distributions or analysis that rely heavily on the low momentum hadrons. Moreover, the parameters used in the simulation are those given by the authors. No attempt has been made to alter any to them in order to gain better agreement between the model and the data.

VITA

Gregory M. Swider

Born: 17 January, 1953 Chicago, Illinois
to Raymond J. Swider and Marguerite (Beiger) Swider

High School: Proviso West High School, Hillside Illinois

Bachelor of Arts: Knox College, Galesburg, Illinois June 1975

Master of Science: University of Washington August 1976

Doctor of Philosophy: University of Washington December 1983